

This is the peer-reviewed version of the article:

Ristić, P.; Blagojević, V.; Janjić, G.; Rodić, M.; Vulić, P.; Donnard, M.; Gulea, M.; Chylewska, A.; Makowski, M.; Todorović, T.; Filipović, N. Influence of C–H/X (X = S, Cl, N, Pt/Pd) Interactions on the Molecular and Crystal Structures of Pt(II) and Pd(II) Complexes with Thiomorpholine-4-Carbonitrile: Crystallographic, Thermal, and DFT Study. *Crystal Growth & Design* 2020, 20 (5), 3018–3033. <https://doi.org/10.1021/acs.cgd.9b01661>



This work is licensed under

[Attribution-NonCommercial 4.0 International license \(CC BY-NC 4.0\)](https://creativecommons.org/licenses/by-nc/4.0/)

1  
2  
3 **1 The influence of C–H/X (X = S, Cl, N, Pt/Pd) interactions on the molecular**  
4 **and crystal structures of Pt(II) and Pd(II) complexes with**  
5 **2 thiomorpholine-4-carbonitrile: crystallographic, thermal and DFT study**  
6  
7  
8  
9

10 4 Predrag Ristić<sup>a</sup>, Vladimir Blagojević<sup>b</sup>, Goran V. Janjić<sup>c</sup>, Marko V. Rodić<sup>d</sup>, Predrag Vulić<sup>e</sup>,  
11 5 Morgan Donnard<sup>f</sup>, Mihaela Gulea<sup>g</sup>, Agnieszka Chylewska<sup>h</sup>, Mariusz Makowski<sup>h</sup>,  
12 6 Tamara R. Todorović<sup>a</sup>, Nenad R. Filipović<sup>i,\*</sup>  
13  
14  
15  
16 7

17  
18 8 *<sup>a</sup> University of Belgrade - Faculty of Chemistry, Studentski trg 12-16, 11000 Belgrade, Serbia*

19  
20 9 *<sup>b</sup> Institute of Technical Sciences of the Serbian Academy of Sciences and Arts, Knez Mihailova*  
21 10 *35/IV, 11000 Belgrade, Serbia*

22  
23 11 *<sup>c</sup> Institute of Chemistry, Metallurgy and Technology, University of Belgrade, Njegoševa 12,*  
24 12 *11000 Belgrade, Serbia*

25  
26 13 *<sup>d</sup> Department of Chemistry, Faculty of Sciences, University of Novi Sad, Trg Dositeja*  
27 14 *Obradovića 4, 21000 Novi Sad, Serbia*

28  
29 15 *<sup>e</sup> Faculty of Mining and Geology, University of Belgrade, Đušina 5, 11000 Belgrade, Serbia*

30  
31 16 *<sup>f</sup> Université de Strasbourg, Université de Haute-Alsace, CNRS, LIMA – UMR 7042, ECPM,*  
32 17 *67000 Strasbourg, France*

33  
34 18 *<sup>g</sup> Université de Strasbourg, CNRS, LIT – UMR 7200, Faculty of Pharmacy, 67000 Strasbourg,*  
35 19 *France*

36  
37 20 *<sup>h</sup> Faculty of Chemistry, University of Gdansk, Wita Stwosza 63, PL80-308 Gdansk, Poland*

38  
39 21 *<sup>i</sup> University of Belgrade - Faculty of Agriculture, Nemanjina 6, 11000 Belgrade, Serbia*

40  
41 22  
42  
43  
44  
45 23 *\*Corresponding author: Nenad R. Filipović, PhD, Associate Professor, University of*  
46 24 *Belgrade - Faculty of Agriculture, Nemanjina 6, 11000 Belgrade, Serbia; E-mail:*  
47 25 *nenadf@agrif.bg.ac.rs*  
48  
49  
50  
51  
52  
53  
54  
55  
56  
57  
58  
59 26  
60

## 1 **Abstract**

2 Pt(II) and Pd(II) complexes (**1** and **2**, respectively) with thiomorpholine-4-carbonitrile (TM-  
3 CN), N-substituted thiomorpholine derivative, were synthesized from tetrachlorido precursors  
4 in water. Structural analysis has shown that **1** represents the first monomeric metal complex  
5 with this ligand type with axial M–S bond with respect to the TM–CN ring chair  
6 conformation, while in **2** a typical equatorial M–S bond position with respect to the ring chair  
7 conformation was observed. A detailed DFT investigation revealed that axial conformers are  
8 more stable for molecular forms of both metals, while intermolecular interactions in the  
9 crystals stabilize the axial conformer for Pt(II) and the equatorial one for Pd(II). The  
10 magnitude of this stabilization in the case of **2** is large enough to change the most stable axial  
11 conformer in the molecular form to the equatorial one in the crystal. Further investigation of  
12 strength of individual intermolecular interactions revealed significant differences of some  
13 interactions between the two structures. The likely cause of the difference in the crystal  
14 structures of experimentally obtained complexes is the fact that **1** and **2** exhibit different  
15 dominant interactions: C–H/M and C–H/S are more dominant in **1** and C–H/Cl interactions  
16 are more dominant in **2**. In addition, DFT calculations have shown that while axial position of  
17 Pt–S bond with respect to the ring chair conformation results in significantly shorter C–H/Pt  
18 interaction distance than in the hypothetical equatorial conformer, there is very little  
19 difference in C–H/Pd interaction distances in conformers with axial and equatorial position of  
20 Pd–S bond with respect to the ring chair conformation.

21

22 **Keywords:** Pd(II) and Pt(II) complexes; periodic DFT; Hirshfeld analysis; intermolecular  
23 interaction energies.

24

25

26

27

28

29

30

31

32

## 1 INTRODUCTION

2 Thian (TH) is a simple monodentate sulfur-containing six-membered heterocyclic  
3 ligand, which can coordinate to metals forming axial or equatorial M–S bonds with respect to  
4 the ring chair conformation. Due to 1,3-diaxial interactions, which contribute to the higher  
5 energy of the axial conformer relative to the equatorial one, a formation of equatorial M–S  
6 bond with respect to the ring chair conformation is preferable. This is in line with the results  
7 of Cambridge Crystallographic Database (CSD) search where, out of 13 reported crystal  
8 structures, there is no crystal structure with exclusively axial position of M–S bond with  
9 respect to the TH ring chair conformation (Table 1).<sup>1</sup> In 11 structures M–S bond is in  
10 equatorial position, while in the case of four complexes sulfur atom coordinates as a double  
11 donor with formation of both axial and equatorial M–S bonds with respect to the TH ring  
12 chair conformation.

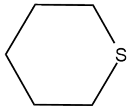
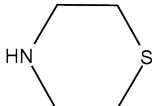
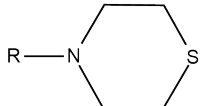
13 Introduction of a nitrogen donor in TH ring results in another heterocyclic sulfur-  
14 based ligand – thiomorpholine (TM). There have been 12 crystal structures of TM complexes  
15 deposited in the CSD (Table 1).<sup>1</sup> Three binding modes are observed for TM: monodentate N  
16 (n-N), bidentate bridging-N ( $\mu$ -N) and tridentate bridging-S (n-N: $\mu$ -S). The latter  
17 coordination mode includes both axial and equatorial position of the M–S bond (where S is  
18 the bridging sulfur atom) with respect to a ring chair conformation, and it was only observed  
19 in the case of one Cu-based TM complex. TM could act as N,S bidentate chelator but this is  
20 unfavorable since boat conformation would be required for the chelating coordination mode.<sup>2</sup>  
21 There have been no reported crystal structures where TM is coordinated to metal exclusively  
22 *via* sulfur atom.

23 *N*-substituted TM analogues (*N*-TMs) have also been used for preparation of metal  
24 complexes and there are currently 18 reported crystal structures deposited in the CSD (Table  
25 1).<sup>1</sup> Coordination modes of *N*-TMLs observed in the crystal structures of the complexes are:  
26 monodentate coordination *via* S atom, mixed N,S chelation and coordination of N atom  
27 together with other donor atoms from R substituent. Exclusive coordination *via* the sulfur  
28 atom was observed in the case of polymeric Cu complexes where ligands contain electron-  
29 withdrawing amide groups bonded to *N*-TMLs.<sup>3–6</sup> A typical, exclusive axial conformer was  
30 observed only in the case of two Cu(I) coordination polymers.<sup>4,7</sup> It is worth mentioning that  
31 in the mixed *N,S* bidentate chelates, *N*-TMs coordinates in the higher energy boat  
32 conformation. There have been several reports on possible application of metal complexes  
33 with *N*-TMs. A comparative study of catalytic activity of Cu(II) binuclear complexes with  
34 phenol-based ligand with *N*-(2-aminoethyl)thiomorpholine side arms, as well as its

1 morpholine and piperidine analogues, showed that TM-based complex is the most active and  
2 potent catechol oxidant.<sup>8</sup> Also, two Ru-based complexes with thioamide-based ligands  
3 showed potential to be used as detectors for NO due to directly observed fluorescence after  
4 NO binding to the metal center.<sup>9</sup> Finally, 2-(cyclohexylthio)-1-thiomorpholinoethanone  
5 ligand forms three Cu(I) coordination polymers which undergo crystal-to-crystal  
6 transformation with and without solvent, while variations of the distance between copper  
7 atoms with temperature are responsible for the observed luminescence thermochromism.<sup>3</sup>

8 Taking into account that many properties of chemical systems are defined not only by  
9 the molecular structure, but also by weak intermolecular interactions<sup>10-15</sup> we found it  
10 interesting to study coordination ability of one unexplored *N*-TM ligand, thiomorpholine-4-  
11 carbonitrile (TM-CN) towards Pd(II) and Pt(II). Both chosen ions have d<sup>8</sup> electronic  
12 configuration and almost the same ionic radii, thus their complexes with the same ligand  
13 systems are often isostructural. However, extended electronic density and higher basicity of  
14 5d Pt(II) ion in comparison to 4d Pd(II) ion, results in stronger M···H–X (X = C, N or O)  
15 interactions for Pt(II) which lead to difference in the structure of the complexes.<sup>16</sup> Thus, these  
16 two systems provide an excellent opportunity to study the effect of intermolecular  
17 interactions on the stability of molecular and crystal structures, given that four different types  
18 of intermolecular interactions can be formed. We present two non-isostructural square-planar  
19 Pd(II) and Pt(II) complexes with TM-CN ligand, showing the difference in the M–S bond  
20 position with respect to the ring chair conformation. To understand the difference in the  
21 crystal structure of synthesized complexes, DFT calculations of TM-CN coordination in a  
22 molecular structure, Hirshfeld surface and fingerprint plot analysis, DFT calculations of  
23 periodic structures with comparison of intermolecular interaction energies, crystallographic  
24 and quantum chemical analysis of observed interactions, as well as detailed thermal stability  
25 investigations were performed.

1  
2  
3 Table 1. Coordination modes of TH, TM and N-TM ligands in crystal structures of complexes  
4 deposited in the CSD  
5  
6

Ligand	TH	TM	N-TM
			
Number of crystal structures	13	12	18
S-eq	Fe, Os, Pd, W, Nb <sup>a</sup> , Ta <sup>a</sup> , Ru	/	Cu
S-ax	/	/	Cu
S-bridging	W, Os, Nb <sup>a</sup> , Ta <sup>a</sup>	/	/
N-monodentate	/	Pd, Co, Ni, Cu, Al	/
N <sup>b</sup>	/	/	Zn, Cu, Pd, Ni
N-bridging	/	Al	/
tridentate bridging S	/	Cu	/
N,S-bis bidentate	/	/	Pd, Rh
N,S-bidentate	/	/	Pd

3 <sup>a</sup>Complexes with two TH ligands with different coordination modes; <sup>b</sup>polydentate coordination *via* N of TM  
4 ring and other donor atoms from R groups.  
5  
6  
7  
8  
9  
10  
11  
12

## EXPERIMENTAL SECTION

### *Materials and Methods*

All the employed reagents and solvents were of analytical grade and used without further purification.  $K_2[PdCl_4]$  ( $\geq 99.9\%$ ) and  $K_2[PtCl_4]$  (98 %) were obtained from Sigma-Aldrich. Elemental analyses (C, H, N, S) were performed by standard micro methods using the ELEMENTARVario ELIII C.H.N.S=O analyzer. The vibrational spectra were recorded by Spectrum Two instrument (Perkin Elmer) in the wavenumber range 4000–450  $cm^{-1}$ , as well as in the range 600–300  $cm^{-1}$  using the Universal Attenuated Total Reflection (UATR) technique. The method used was insensitive to samples thickness or shape due to the presence of the UATR hard crystal material. The apparatus was equipped by a diamond material with the measurable surface of about 4  $mm^2$  allowing good contact with both samples. Molar conductivity measurements were performed at ambient temperature (298 K) on the Crison Multimeter MM41. The NMR spectral measurements were performed on a Bruker Avance III 500 spectrometer or Agilent 400-MR spectrometer equipped with a broad-band direct probe. The spectra were recorded at room temperature in  $DMSO-d_6$ ,  $CDCl_3$  or  $CD_3NO_2$ . Chemical shifts are given on  $\delta$  scale relative to tetramethylsilane as internal standard for  $^1H$  and  $^{13}C$ . Assignments of signals in NMR spectra are given in ESI. High resolution electron spray ionization mass spectrum (HRMS-ESI) of the ligand was recorded on a Agilent Technologies 6210-1210 TOF-LC-ESI-MS instrument operating in the positive ion mode. The thermogravimetric analysis was performed by means of thermal equalizer TG209 Nietzsche coupled with FT-IR. The analyzer was equipped with a programmable temperature controller, which automatically maintains constant temperature during thermal events. The TG weight-loss measurements were performed in 20–950  $^{\circ}C$  temperature range at a heating rate of 15 $^{\circ}C/min$ , in alumina crucible. The IR spectra were of gaseous decomposition products were registered using a Bruker IFS 66 spectrophotometer. All experiments were carried out in an argon atmosphere and verified at least twice.

### *Synthesis of the ligand thiomorpholine-4-carbonitrile (TM-CN)*

The ligand was synthesized according to the literature procedure.<sup>17</sup> White solid; m.p.: 41–43  $^{\circ}C$ . Anal Calcd. for  $C_5H_8N_2S$  ( $MW = 128.20$ ): C, 46.85; H, 6.29; N, 21.85; S, 25.01. Found: C, 46.97; H, 6.43; N, 21.77; S, 24.96 %.  $^1H$  NMR ( $CDCl_3$ , 500.26 MHz)  $\delta_H$ : 2.70 (t, 4H), 3.46 (t, 4H);  $^{13}C$  NMR ( $CDCl_3$ , 126 MHz)  $\delta_C$ : 26.1, 50.8, 117.4. HRMS (ESI) m/z calcd. for  $C_5H_9N_2S$  (M+H)<sup>+</sup> 129.0481, found 129.0478.

### 1 **Synthesis of [PtCl<sub>2</sub>(TM-CN)<sub>2</sub>] (1)**

2 Solid K<sub>2</sub>[PtCl<sub>4</sub>] (0.081 g, 0.2 mmol) was added into the solution of TM-CN (0.050 g,  
3 0.390 mmol) in H<sub>2</sub>O (10 mL). A pale-yellow precipitate formed immediately. Reaction  
4 mixture was stirred at 50 °C for 1 h, after which the precipitate was separated by filtration,  
5 washed with small portions of cold H<sub>2</sub>O and EtOH and dried in desiccator. Yield: 0.091 g  
6 (90 %). Quality single crystals were obtained by slow diffusion of EtOH vapor into the  
7 DMSO solution of the product. Anal. Calcd. for C<sub>10</sub>H<sub>16</sub>Cl<sub>2</sub>N<sub>4</sub>PtS<sub>2</sub> (*MW* = 522.38): C, 22.99;  
8 H, 3.09; N, 10.73; S, 12.27 %. Found: C, 22.78; H, 3.15; N, 10.74; S, 12.48.  $\Lambda_M$  (1 ×  
9 10<sup>-3</sup> M, MeCN) = 18.2 Ω<sup>-1</sup> cm<sup>2</sup> mol<sup>-1</sup>.

### 10 **Synthesis of [PdCl<sub>2</sub>(TM-CN)<sub>2</sub>] (2)**

11 Solid K<sub>2</sub>[PdCl<sub>4</sub>] (0.050 g, 0.15 mmol) was added into the solution of TM-CN (0.010  
12 g, 0.075 mmol) in H<sub>2</sub>O (10 mL). Reaction mixture was stirred at 50 °C for 1 h. The yellow  
13 colored precipitate was separated under the vacuum and dried in the desiccator. Yield: 0.024  
14 g (72%). Quality single crystals were obtained by slow diffusion of pentan-2-one vapor into  
15 the nitromethane solution of the product. After two days yellow single crystals were filtered  
16 off and washed with cold water. Anal. Calcd. for C<sub>10</sub>H<sub>16</sub>Cl<sub>2</sub>N<sub>4</sub>PdS<sub>2</sub> (*MW* = 433.69): C, 27.69;  
17 H, 3.72; N, 12.92; S, 14.78 %. Found: C, 27.48; H, 3.59; N, 12.74; S, 14.84.  $\Lambda_M$  (1 ×  
18 10<sup>-3</sup> M, MeCN) = 10.10 Ω<sup>-1</sup> cm<sup>2</sup> mol<sup>-1</sup>.

### 19 **X-ray crystallography**

20 Single crystal X-ray diffraction was performed on an Oxford Diffraction Gemini S  
21 kappa geometry diffractometer, equipped with Mo K $\alpha$  radiation ( $\lambda$  = 0.71073 Å) from a  
22 sealed tube source, and a Sapphire CCD detector. Data collection strategy calculation, data  
23 reduction, cell refinement and absorption correction were performed with the  
24 CRYCALISPRO.<sup>18</sup> Structures were solved using SHELXT<sup>19</sup> and refined with anisotropic  
25 displacement parameters for all non-hydrogen atoms using SHELXL-2014/6.<sup>20</sup> Program  
26 SHELXLE<sup>21</sup> was used as graphical user interface for structure solution and refinement  
27 procedures. Hydrogen atoms bonded to carbon atoms in **1** and **2** were introduced in idealized  
28 positions and refined using riding model structures were validated using PLATON<sup>22</sup> and CSD  
29 (v. 5.40, updates Aug. 2019)<sup>23</sup> using MERCURY CSD.<sup>24</sup>

30 The X-ray powder diffraction (XRPD) investigation was conducted on Rigaku  
31 Smartlab X-ray Diffractometer in  $\theta$ - $\theta$  geometry (the sample in horizontal position) in  
32  
33



1  
2  
3 1 parafocusing Bragg-Brentano geometry using D/teX Ultra 250 strip detector in 1D standard  
4 2 mode with  $\text{CuK}_{\alpha 1,2}$  radiation source ( $U = 40$  kV and  $I = 30$  mA). The XRPD patterns were  
5 3 collected in  $5\text{--}65^\circ 2\theta$  range, with step of  $0.01^\circ$ , and data collection speed of  $5^\circ/\text{min}$  with  
6 4 horizontal sample rotation of 20 rpm. For every sample small amount of single crystals was  
7 5 pulverized, and low background single crystal silicon sample holder was used to minimize  
8 6 the background. The crystal phases present in the samples were identified in dedicated  
9 7 Rigaku PDXL 2.0 software, comparing them with user database compromised of  
10 8 crystallographic information files (CIF) previously obtained by single crystal X-ray  
11 9 diffraction (SC XRD) structure determination.  
12  
13  
14  
15  
16  
17  
18  
19  
20

### 21 ***DFT calculations***

22  
23 12 Geometry optimization of individual molecules was performed using Gaussian09  
24 13 software,<sup>25</sup> with WB97XD method, 6-31+G\*\* basis set for non-metals (C, H, N, S, and Cl)  
25 14 and LANL2DZ for metal ions (Pd and Pt) and SMD solvation model.<sup>26</sup> Lack of imaginary  
26 15 frequency in the frequency calculation was taken as a confirmation of a true minimum. DFT  
27 16 calculations on a periodic system were conducted on a unit lattice using ABINIT 8.10  
28 17 software package<sup>27</sup> with PBE0 functional<sup>28</sup> and norm-conserving ONCVSP-3.2.3.1  
29 18 pseudopotential. Energy cutoff was 990 eV and SCF tolerance was  $5 \times 10^{-7}$  eV per atom.

30 19 To get insight into the strength of particular interactions involving in crystal packing  
31 20 of the considered complexes (C–H/Cl–M, C–H/S–M, C–H/N $\equiv$ C and C–H/M interactions),  
32 21 DFT calculations on a model system  $\text{CH}_4/\text{metal}$  complex were performed. Unlike the  
33 22 previous set of calculations, these were conducted only on the equatorial conformers, because  
34 23 it provided the best model where these specific interactions could be isolated by eliminating  
35 24 any chance of potential additional interactions of the TM–CN ligand and  $\text{CH}_4$ . Therefore,  
36 25 only structures with equatorial M–S bonds with respect to the ring chair conformation were  
37 26 used in the calculation. During these calculations the distance of H atom to the corresponding  
38 27 acceptor atom (Cl, S, N, Pt, and Pd) is changed in range from 2.5 to 3.5 Å.  
39  
40  
41  
42  
43  
44  
45  
46  
47  
48  
49  
50  
51  
52

### 53 29 ***Hirshfeld surface analysis and calculation of intermolecular interaction energies***

54 30 For visualization of Hirshfeld surfaces, CIF files were used. Hirshfeld surfaces  
55 31 visualization and presentation of results as  $d_{\text{norm}}$ , shape index and curvedness as well as  
56 32 calculation of 2D fingerprint plots with  $d_e$  and  $d_i$  distances were generated using Crystal  
57 33 Explorer v.17.5.<sup>29,30</sup> The distance from the surface to the nearest nucleus of the atom on the

1  
2  
3 1 outside of the surface is denoted as  $d_e$  while the distance from the surface to the closest  
4  
5 2 nucleus of the atom on the inside of the surface is denoted as  $d_i$ . Surfaces are mapped over a  
6  
7 3 standard color scale and 2D fingerprint plots are calculated using  $d_e$  and  $d_i$  values in the range  
8  
9 4 0.4–2.8 Å.

10 5 Intermolecular interaction energies were calculated using CrystalExplorer v17.5, with  
11  
12 6 wavefunction calculated using Gaussian09 software<sup>25</sup> with B3LYP method, 6-31G(d,p) basis  
13  
14 7 set for non-metals (C, H, N, S, and Cl) and DGDZVP for metal center.  
15  
16 8

### 17 9 ***Crystallographic analysis of X–H/Cl–M, X–H/S–M, X–H/M, and X–H/N≡C interactions***

18  
19 10 The crystallographic analysis of X–H/Cl–M, X–H/S–M, X–H/M, and X–H/N≡C  
20  
21 11 interactions is based on the crystal structures extracted from the CSD.<sup>31</sup> The study  
22  
23 12 of X–H/M interactions is based on structures with M ion from square-planar complexes. The  
24  
25 13 geometric parameters used for search the CSD were the same for all analyzed interactions:  
26  
27 14 distance between H atom from X–H group and acceptor atom (A= Cl, S or M) is less than 2.9  
28  
29 15 Å (H⋯A or d distance) and X–H⋯A angle ( $\alpha$  angle) is larger than 110°. Analyzed structures  
30  
31 16 had to satisfy the following criteria: (a) the crystallographic  $R$  factor less than 10%; (b) error-  
32  
33 17 free coordinates according to the criteria used in the CSD system; (c) no crystallographic  
34  
35 18 disorder; (d) no polymeric structures; (e) positions of all hydrogen atoms normalized.

## 36 19 **RESULTS AND DISCUSSION**

### 37 38 20 ***Synthesis and characterization of the complexes***

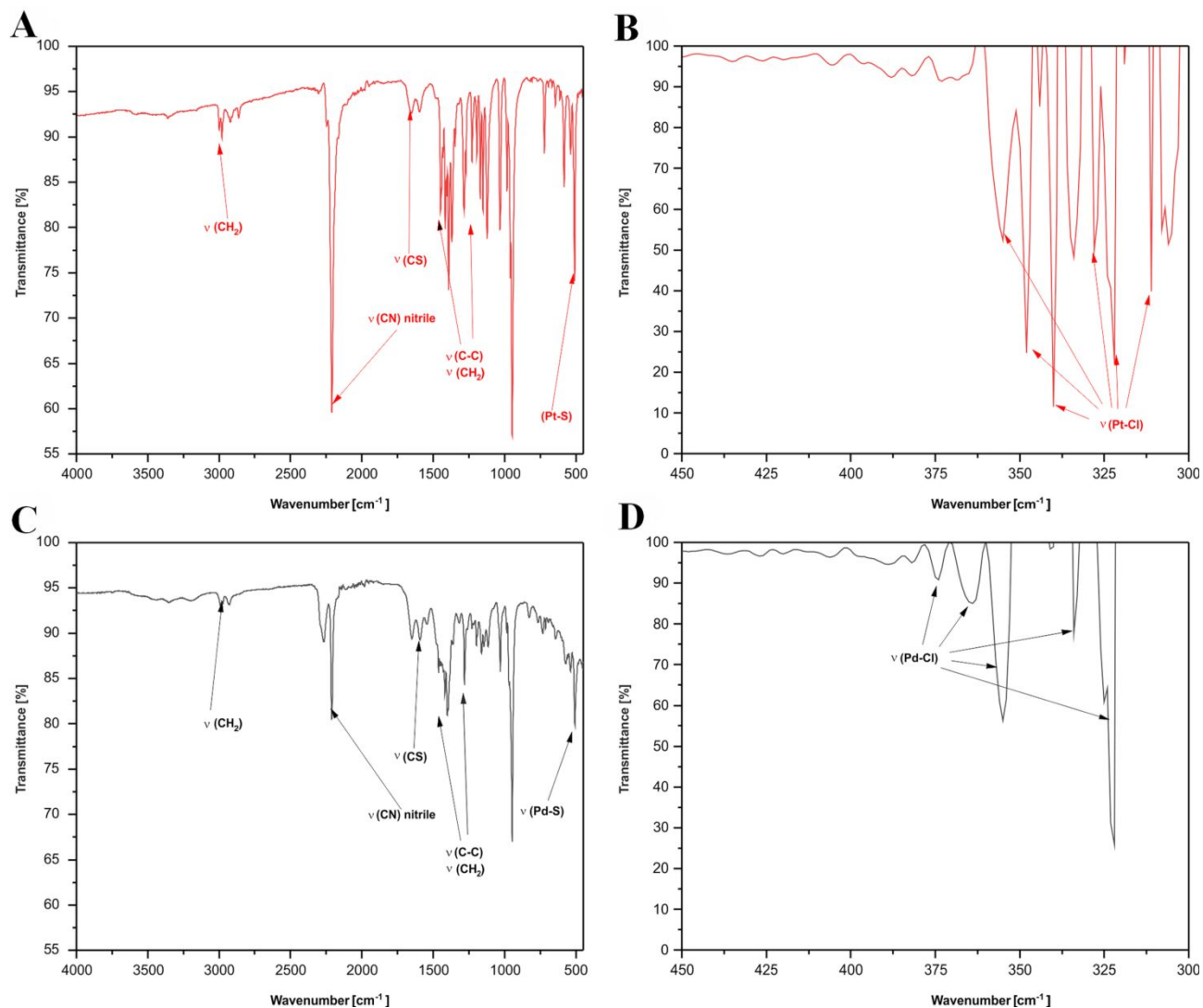
39  
40 21 The complexes were obtained by reaction of TM–CN with  $K_2[MCl_4]$  (M = Pt or Pd)  
41  
42 22 in water as a solvent in a molar ratio ligand : metal salt = 2 : 1. Pale yellow (Pt-complex **1**)  
43  
44 23 and orange (Pd-complex **2**) precipitates were obtained after 1 h at 50 °C. Single crystals  
45  
46 24 suitable for X-ray diffraction (XRD) analysis (*vide infra*) were obtained by a vapor diffusion  
47  
48 25 method. Results of elemental analysis indicate that molar ratio of the ligand and metal ions is  
49  
50 26 preserved in the obtained complexes, therefore the complexes can be represented by the  
51  
52 27 following general formula  $[MCl_2(TM-CN)_2]$  (M = Pt, Pd). They are soluble in DMSO,  
53  
54 28 DMF, MeCN and MeNO<sub>2</sub>, and sparingly soluble in MeOH and EtOH. Molar conductivity  
55  
56 29 measurements for both compounds were performed in MeCN solution. Obtained values are  
57  
58 30 lower than those characteristic for 1:1 electrolytes, indicating that molecular complexes were  
59  
60 31 obtained, which is in agreement with the proposed general formula.

The detailed assignment of vibrations of **1** and **2**, with corresponding mode descriptions, are reported in Table S1, Electronic Supplementary Material (ESI). Methylene ( $\text{CH}_2$ ) group vibrations of TM–CN ligand in both complexes are observed as intense peaks in the range 2900–3000  $\text{cm}^{-1}$  (Figure 1), originating from the overlapping of the absorption peaks of symmetric and asymmetric stretching of the  $\text{CH}_2$  group in the coordinated ligand.<sup>32,33</sup> Additionally, these stretching frequencies are associated with vibrational modes like rocking and twisting, as well as wagging modes related with polarization of vibrations.<sup>34</sup> The  $\text{CH}_2$ -stretching region of coordinated TM–CN ligand in the complexes is surprisingly similar to coordinated morpholine or piperazine, with the exception of changes in relative intensities. This suggests that the lone pair orbitals on sulfur may play a similar role to that of oxygen or nitrogen in shifting the position of certain  $\text{CH}_2$  bands.<sup>35</sup> Among the other vibrations of  $\text{CH}_2$  group of TM–CN ligand in both complexes, the bands at 1280–1113  $\text{cm}^{-1}$  region are related to wagging, and twisting. In addition, rocking modes of  $\text{CH}_2$  group at 980  $\text{cm}^{-1}$  are also observed.<sup>36</sup> The other bands of  $\text{CH}_2$  group are observed in the expected region and are presented in Table S1 (ESI). Moreover, the UATR bands of ring vibrations are identified in 1283–1113, 980–740 and 580–540  $\text{cm}^{-1}$  regions as very weak and weak peaks for **2** and medium strong and strong peaks for **1**. The lower frequencies of these peaks in comparison to the free ligand are probably due to the coordination of TM–CN ligand to the metal centers.<sup>37</sup>

The absorption region between 2260 and 2200  $\text{cm}^{-1}$  is assigned to the stretching vibrations of  $\text{C}\equiv\text{N}$  group. In IR spectra of the complexes, the  $\text{C}\equiv\text{N}$  stretching bands are very intense, although the peak observed for **1** is more intense than that of **2**. The in-plane bending of N–CN bond is obtained in the low frequency regions at 540  $\text{cm}^{-1}$  and 543  $\text{cm}^{-1}$  for **1** and **2**, respectively, overlapping with C–C in-plane bending vibration. Thiols or thioamides generally exhibit IR absorption at 1750–1400  $\text{cm}^{-1}$ ,<sup>38</sup> with ring size, metal ionic center bound, steric and electric effects resulting in significant shifts in CS absorption frequencies.<sup>39</sup> In **1** (Figure 1A) and **2** (Figure 1C) the C–S stretching vibrations are observed in 1652–1401  $\text{cm}^{-1}$  for both compounds. Additionally, the intense peaks observed in 505  $\text{cm}^{-1}$  for **1** and 504  $\text{cm}^{-1}$  for **2** are assigned to the stretching vibrations of M–S bonds.

Square-planar complexes **1** and **2**,  $\nu(\text{M–Cl})$  are sensitive to the ligand's *trans*-influence,<sup>40</sup> which has been studied extensively using UATR spectroscopy. Vibrational spectra of *trans* isomers of **1** and **2** exhibit several  $\nu(\text{M–Cl})$  band in the infrared below 400  $\text{cm}^{-1}$ . Additionally, the UATR spectra of **1** (Figure 1B) and **2** (Figure 1D) appear to confirm

1 the stereochemistry of these compounds, as well as indicate the presence of M–Cl bonds  
 2 inside the coordination spheres of both compounds (Table S1, ESI).



5 Figure 1. UATR spectra in the 4000–450  $\text{cm}^{-1}$  region of *trans*-[PtCl<sub>2</sub>(TM-CN)<sub>2</sub>] (**1**) (A) and  
 6 *trans*-[PdCl<sub>2</sub>(TM-CN)<sub>2</sub>] (**2**) (C). UATR spectra in the 450–300  $\text{cm}^{-1}$  region of **1** (B) and **2**  
 7 (D).

### 9 *Thermal behavior*

10 Thermal analyses of **1** and **2** were carried out by the TG and DTG techniques. The  
 11 volatile products of the early stages of decomposition were collected and identified by IR  
 12 spectroscopy. The experimental results for both compounds studied revealed that the

1 degradation occurred in three main steps (Figure 2). The study of thermal decomposition of **1**  
2 indicated its increased heat endurance. It decomposed in temperatures range 170–730 °C.  
3 Both complexes are stable up to about 170 °C. Above this temperature, the elimination of the  
4 greatest part of TM–CN begins. The temperature ranges and the relative observed and  
5 calculated weight losses are given in Table 2. From the weight loss the stoichiometries of the  
6 resultant intermediate species are assigned. The data corresponds to temperatures between  
7 170 and 725 °C suggest a multi-step decomposition of both compounds. Then a series of  
8 exothermic heat changes, in both cases, corresponds to a complete decomposition of the  
9 residual sulfur-based TM–CN ligand and the formation of PtO and PdO, respectively. A  
10 period of slow losses of weight followed by further losses of chlorides and formation of  
11 oxides was complete by about 725 °C. No metal thiocyanates, sulfides or sulfates were  
12 detected in the course of the decomposition as it was reported in the case of thermal  
13 decomposition of metal chloride thiomorpholine complexes.<sup>41</sup> Based on all this, it can be  
14 concluded that the thermal decompositions of **1** and **2** occur through breaking of metal-sulfur  
15 bonds. The residual masses of 34.10% (PtO) and 36.10% (PdO) for **1** and **2**, respectively,  
16 were caused by simultaneous formation of nitrogen, carbon and sulfur species (NO, CO, CO<sub>2</sub>,  
17 H<sub>2</sub>S) and Cl<sub>2</sub> (Figures S1 and S2, ESI). Moreover, the theoretical (calculated) and  
18 experimental percentages of mass losses of both complexes are in very good agreement  
19 (Table 2).  
20

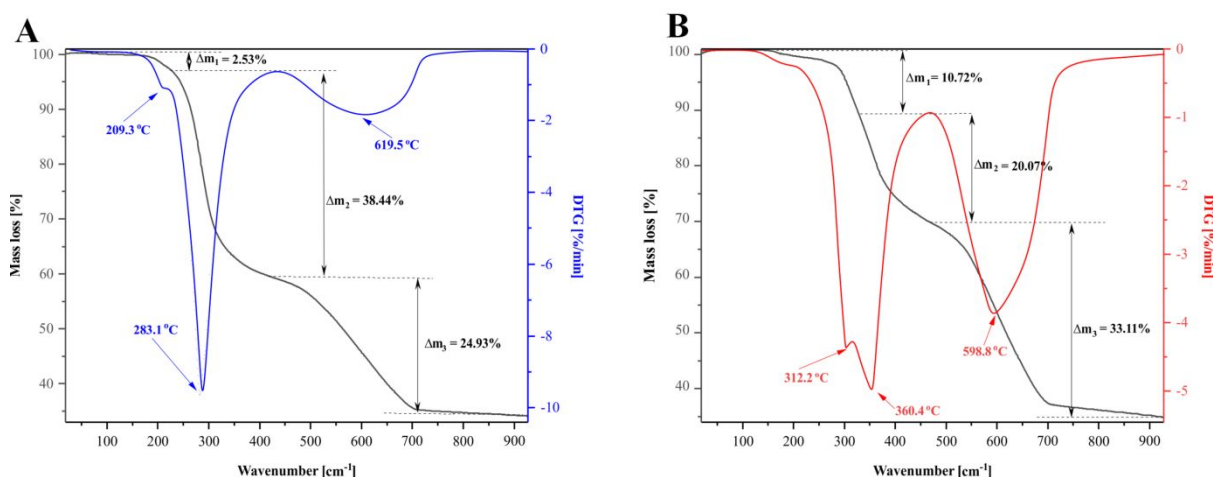


Figure 2. TG and DTG curves of complexes **1** (A) and **2** (B).

1 Table 2. Thermal analysis data for **1** and **2**.

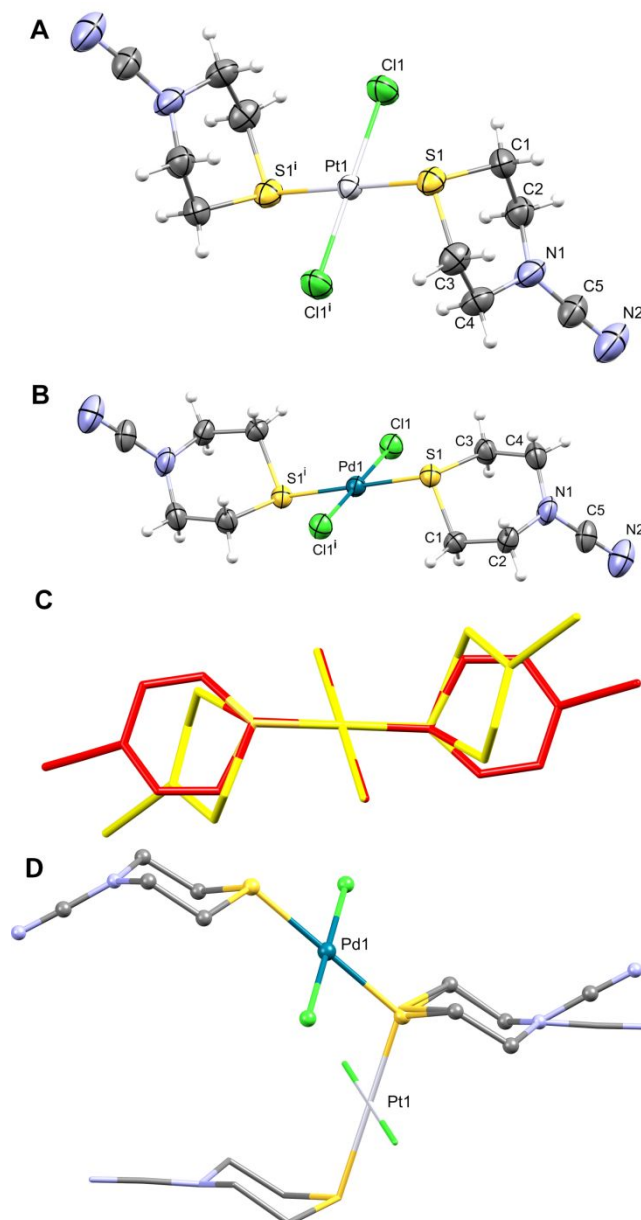
Complex	Step	Onset [°C]	Endset [°C]	Leaving group	Mass loss [%]		Residue
					<i>Exp.</i>	<i>Calc.</i>	Exp. ( <i>Calc.</i> )
<b>1</b>	1	20	250	NH <sub>3</sub>	2.53	3.24	97.47 (96.76)
	2	250	410	CO <sub>2</sub> / NO <sub>2</sub> / H <sub>2</sub> S/ CO	38.44	38.17	59.03 (58.59)
	3	420	725	Cl <sub>2</sub> / CO/ NO	24.93	24.61	PtO 34.10 (33.98)
<b>2</b>	1	20	330	CO <sub>2</sub>	10.72	10.11	89.28 (89.89)
	2	330	475	NO <sub>2</sub> / H <sub>2</sub> S/ NO	20.07	20.99	69.21 (68.90)
	3	475	730	NH <sub>3</sub> / Cl <sub>2</sub> / CO/ NO	33.11	33.56	PdO 36.10 (35.34)

### 4 *XRD analysis*

5 The summary of data collection and refinement parameters for **1** and **2** are given in  
6 Table S2 (ESI), whereas selected bond lengths and bond angles are presented in Table S3  
7 (ESI). The complexes **1** and **2** crystallize in monoclinic crystal system, but in different space  
8 groups (*I2/a* and *P2<sub>1</sub>/c*, respectively). Both complexes are centrosymmetric, with metal ions  
9 residing on a special position with site symmetry  $-1$  (Wyckoff letter *a* for **1** and *d* for **2**).  
10 Thus, asymmetric units of the obtained *trans* isomers consist of a metal center, one TM–CN  
11 coordinated *via* S atom and one chloride ion. Molecular structures of obtained square planar  
12 complexes **1** and **2** are depicted in Figure 3. Although Pt and Pd atoms lie in  $C11, S1, C11^i, S1^i$   
13 plane (**1**:  $i = 1 - x, 1 - y, 1 - z$ ; **2**:  $i = 1 - x, -y, 1 - z$ ) and *trans*-bond angles are exactly 180°,  
14 the coordination geometry around metal centers in both complexes is distorted since *cis*-bond  
15 angles deviate slightly from an ideal value of 90° (Table S3, ESI). Noteworthy, although in  
16 both complexes thiomorpholine rings are in a chair conformation, the position of M–S bonds  
17 with respect to the ring chair conformation is different. In **1**, Pt–S bond is in axial, while Pd–  
18 S bond in **2** is in equatorial position with respect to the ring chair conformation. Overlay of  
19 both structures is depicted in Figure 3C,D. These conformational differences are also  
20 reflected in the values of M–S–Cg angles, where Cg represents a centroid of the  
21 thiomorpholine ring (Table S3, ESI), as well as in the values of the corresponding torsional  
22 angles M–S1–C1–C2 and M–S1–C3–C4 (Table S3, ESI). Due to contribution of a resonance  
23 structure with positive charge on thiomorpholine nitrogen atom ( $+N1=C5=N2^-$ ), CN  
24 substituent in both complexes is bonded to the thiomorpholine ring in a position which is  
25 between axial and equatorial one with respect to the ring chair conformation. This is also

1 reflected in a sum of corresponding bond angles around N1 ( $343.9^\circ$  in **1** and  $359.1^\circ$  in **2**). The  
 2 N–CN fragment is almost linear with N–CN angle of  $178.3^\circ$  in **1** and  $177.5^\circ$  in **2**.

3 Due to similar ionic radii of metal ions,<sup>42</sup> the lengths of the corresponding  
 4 coordination bonds (M–Cl and M–S) are similar in both systems (Table S3, ESI) and are  
 5 typical of values found in related Pt(II) and Pd(II) complexes.<sup>23,43</sup> Lengths of bonds in TM  
 6 ring are also in the usual range.<sup>24,44</sup>



8  
 9  
 10 Figure 3. Perspective view and labeling of molecular structure of **1** (A) and **2** (B). Thermal  
 11 ellipsoids are at the 50% probability level. Equivalent atoms are generated by the  
 12 transformation  $i = 1 - x, 1 - y, 1 - z$  for **1** and  $i = 1 - x, -y, 1 - z$  for **2**. (C) Overlay (through

1  
2  
3 1 M and four donor atoms) of molecular structures of **1** (yellow) and **2** (red). (D) Overlay  
4 (through C1, C2, N1, C3 and C4) of molecular structures of **1** (capped sticks) and **2** (ball and  
5 sticks). Hydrogen atoms are omitted for clarity (C, D).  
6  
7  
8  
9

10 Thiomorpholine methylene groups form intramolecular C–H/Cl and C–H/M  
11 interactions. It is well known that metal complexes can form hydrogen bonds in which metal  
12 ion serves as an acceptor.<sup>44</sup> As a consequence of conformational differences, H···Cl and  
13 H···M distances in the two structures are different and shorter in the system with axial M–S  
14 bonds. In **1**, each Cl ligand forms two C–H/Cl interactions with two methylene groups from  
15 one ligand and one interaction with methylene group from another ligand (**1**: Cl1···H3A =  
16 2.809 Å, Cl1···H4A = 2.764 Å, Cl1···H1B<sup>*i*</sup> = 2.689 Å, *i* = 1 – *x*, 1 – *y*, 1 – *z*). In **2**, one  
17 methylene group from one ligand is involved in bifurcated C–H···Cl interaction, while one  
18 methylene group from other ligand forms one interaction with Cl ligand (**2**: Cl1···H1B =  
19 2.938 Å, Cl1···H3B<sup>*i*</sup> = 2.913 Å, Cl1···H3A<sup>*i*</sup> = 3.088 Å, *i* = 1 – *x*, –*y*, 1 – *z*). Pd(II) forms two  
20 C–H/Pd interactions with one CH<sub>2</sub> group from each ligand, while Pt(II) forms four C–H/Pt  
21 interactions with two CH<sub>2</sub> groups from each ligand (**1**: Pt1···H2B = 3.141 Å, Pt1···H4A =  
22 3.273 Å; **2**: Pd1···H1A = 3.293 Å). Intramolecular interactions are depicted in Figure 4. Such  
23 distribution of intramolecular interactions is a consequence of a difference in the position of  
24 M–S bond (axial or equatorial) with respect to the ring chair conformation of TM–CN.  
25 However, it should be stressed that Pt(II) ion forms somewhat stronger hydrogen bonds than  
26 Pd(II) ion.<sup>44–46</sup> It is also useful to point out that weak C–H hydrogen bonding has the ability  
27 to prevent rotational flexibility of coordinative bonds and conformational flexibility of  
28 ligands.<sup>47</sup>  
29  
30  
31  
32  
33  
34  
35  
36  
37  
38  
39  
40  
41  
42  
43  
44  
45  
46  
47  
48  
49  
50  
51  
52  
53  
54  
55  
56  
57  
58  
59  
60



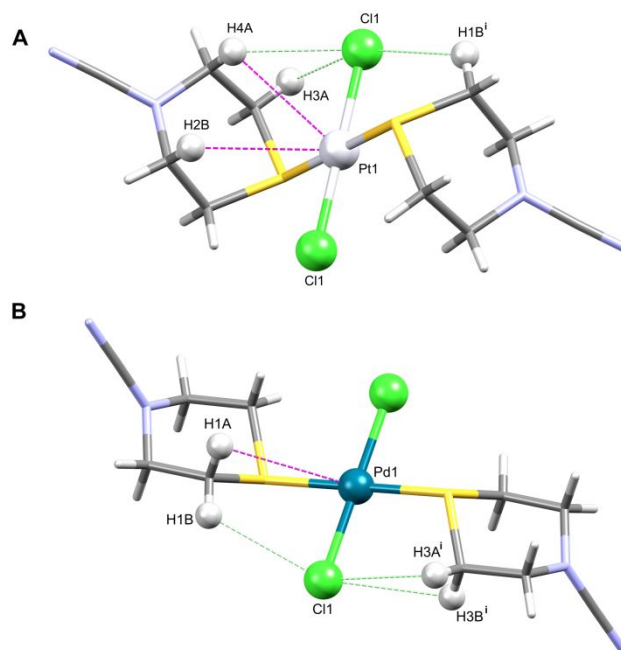


Figure 4. Intramolecular C–H/Cl (blue) and C–H/M (magenta) interactions in molecular structures of **1** (A) and **2** (B). Symmetry operations:  $i = 1 - x, 1 - y, 1 - z$  in **1** and  $i = 1 - x, -y, 1 - z$  in **2**.

The cell packing diagrams for the two complexes is depicted in Figure 5. Due to the absence of a classical proton donor crystal packing in both complexes are based on weak hydrogen bonds.

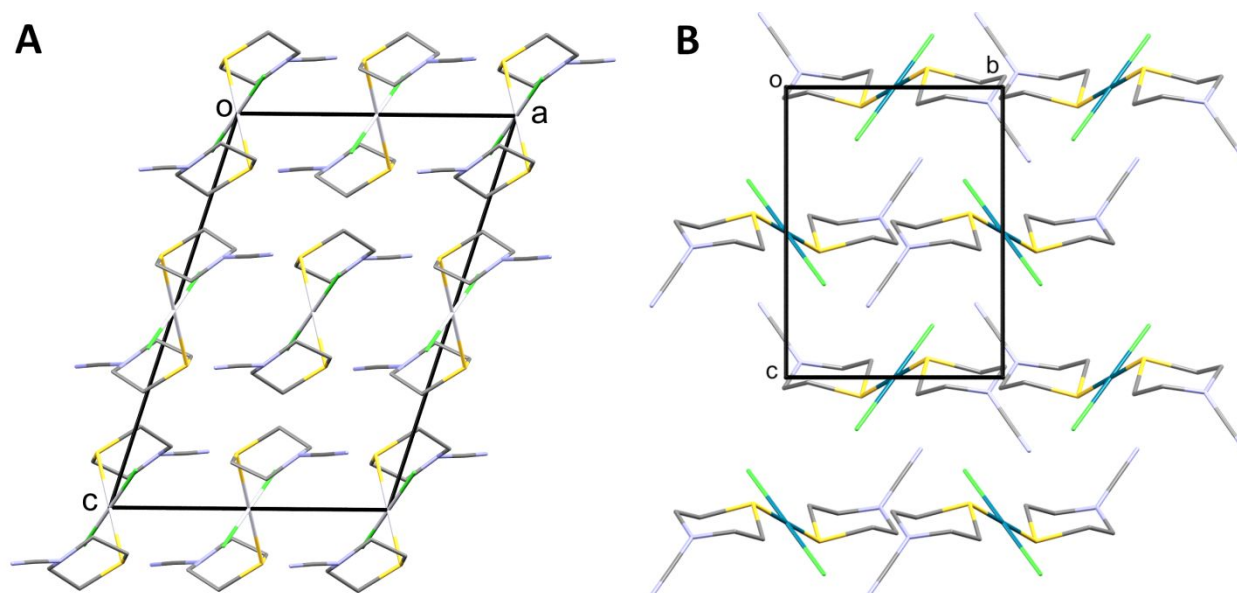
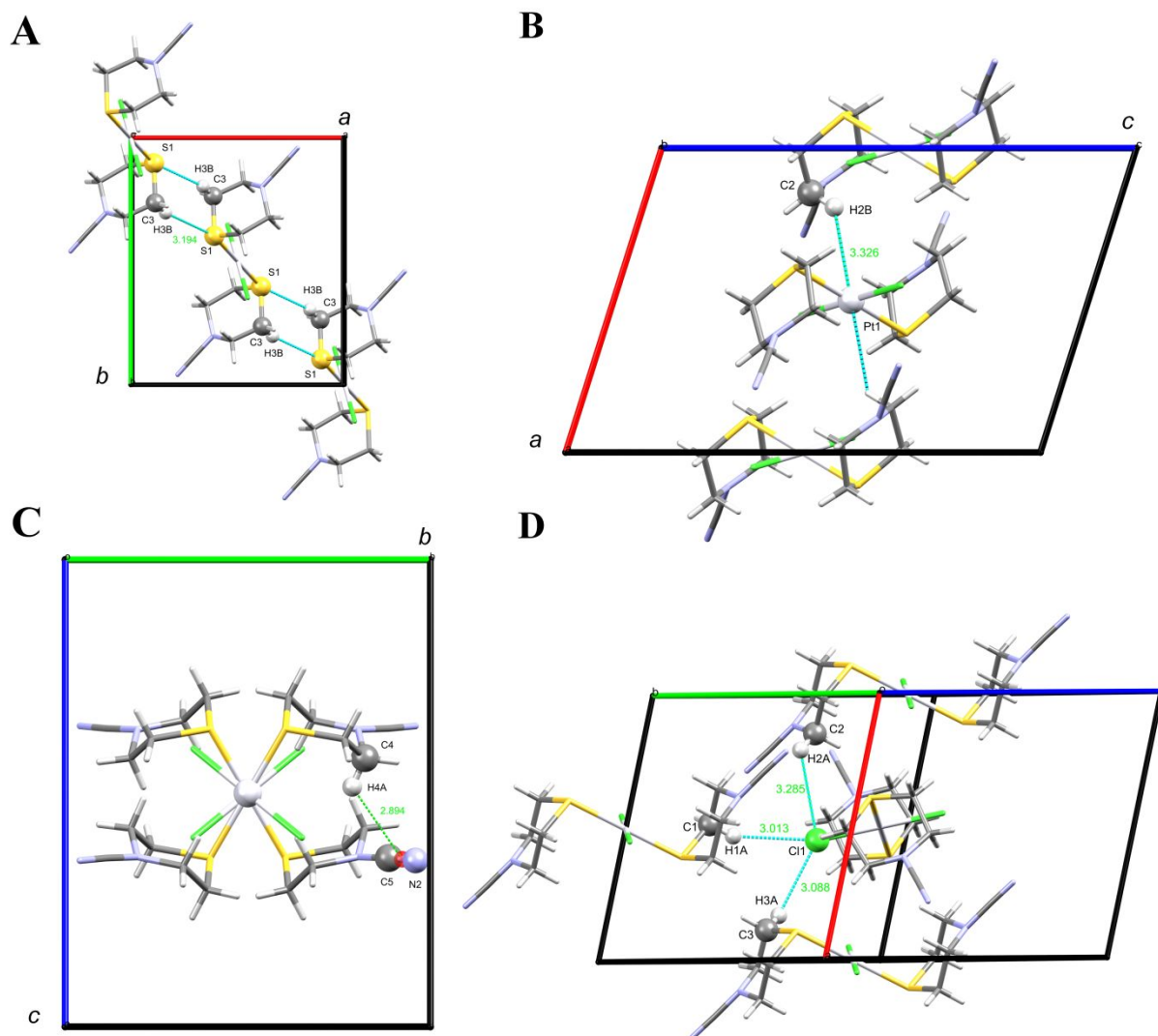


Figure 5. The cell packing diagrams for **1** (A) and **2** (B).

Each molecule of **1** is involved in four C–H/S interactions with two adjacent molecules with a formation of 1-D chains parallel to  $[1\ 1\ 1]$  [ $C3-H3B/S1$  ( $\frac{1}{2} - x, \frac{1}{2} - y, \frac{1}{2} - z$ ) = 4.137 Å,  $C-H\cdots S = 165^\circ$ ] (Figure 6A). Due to space group symmetry the same interactions are responsible for formation of 1-D chains parallel to  $[1\ -1\ 1]$ . These two types of chains are interlinked through C–H/Pt, C–H/Cl and C–H/ $\pi$  interactions, thus forming 3-D crystal packing. Each molecule of Pt(II) complex is involved in four C–H/Pt interactions [ $C2-H2B/Pt1$  ( $1.5 - x, y, 1 - z$ ) = 4.095 Å,  $C-H\cdots Pt = 137.6^\circ$ ] (Figure 6B), C–H/ $\pi$  interactions [ $C4-H4A/Cg$  ( $1.5 - x, y, 1 - z$ ) = 3.520 Å,  $C-H\cdots Cg = 127.19^\circ$ ; Cg is centroid of carbonitrile bond] with adjacent complex molecules (Figure 6C) and three C–H/Cl interactions [ $C1-H1A/Cl1$  ( $x, \frac{1}{2} - y, \frac{1}{2} + z$ ) = 3.894 Å,  $C-H\cdots Cl = 137.6^\circ$ ,  $C2-H2A/Cl1$  ( $1.5 - x, y, 1 - z$ ) = 3.285 Å,  $C-H\cdots Cl = 119.39^\circ$ ,  $C3-H3A/Cl1$  ( $\frac{1}{2} - x, y, 1 - z$ ) = 3.088 Å,  $H\cdots Cl = 122.47^\circ$ ] (Figure 6D).



14

17

1  
2  
3 1 Figure 6. C–H/S (A), C–H/Pt (B), C–H/ $\pi$  (C) and C–H/Cl (D) interactions in the crystal  
4 packing of **1**.  
5  
6  
7  
8  
9

10 4 On the other hand, each molecule of **2** forms four C–H/S interactions with two  
11 adjacent molecules with formation of 2-D layers parallel to (100) [C3–H3B/S1 ( $1 - x, -\frac{1}{2} +$   
12  $y, 1.5 - z$ ) = 3.136 Å, C–H $\cdots$ S = 155.36°] (Figure 7A). Additionally, each complex molecule  
13 6 is involved in four C–H/Pd interactions with two adjacent molecules [C2–H2A/Pd1 ( $x, 1 + y,$   
14 7  $z$ ) = 3.785 Å, C–H $\cdots$ Pd = 140.08°] where in two interactions is hydrogen bond donor and in  
15 8 other two is an acceptor (Figure 7B). Also, each molecule of **2** interacts thorough three C–  
16 9 H/Cl contacts [C1–H1A/Cl1 ( $1 - x, 1 - y, 1 - z$ ) = 2.996 Å, C–H $\cdots$ Cl = 153.78°; C1–  
17 10 H1B/Cl1 ( $x, 1 + y, -1 + z$ ) = 2.858 Å, C–H $\cdots$ Cl = 144.51°; C2–H2A/Cl1 ( $x, 1.5 - y, -\frac{1}{2} - z$ )  
18 11 = 2.888 Å, C–H $\cdots$ Cl = 132.87°] (Figure 7C) and one C–H/ $\pi$  contact [C4–H4A/Cg ( $1 - x, 1 -$   
19 12  $y, -z$ ) = 3.087 Å, C–H $\cdots$ Cg = 132.61°; Cg is centroid of carbonitrile bond] (Figure 7D).  
20  
21  
22  
23  
24  
25  
26  
27  
28  
29  
30  
31  
32  
33  
34  
35  
36  
37  
38  
39  
40  
41  
42  
43  
44  
45  
46  
47  
48  
49  
50  
51  
52  
53  
54  
55  
56  
57  
58  
59  
60

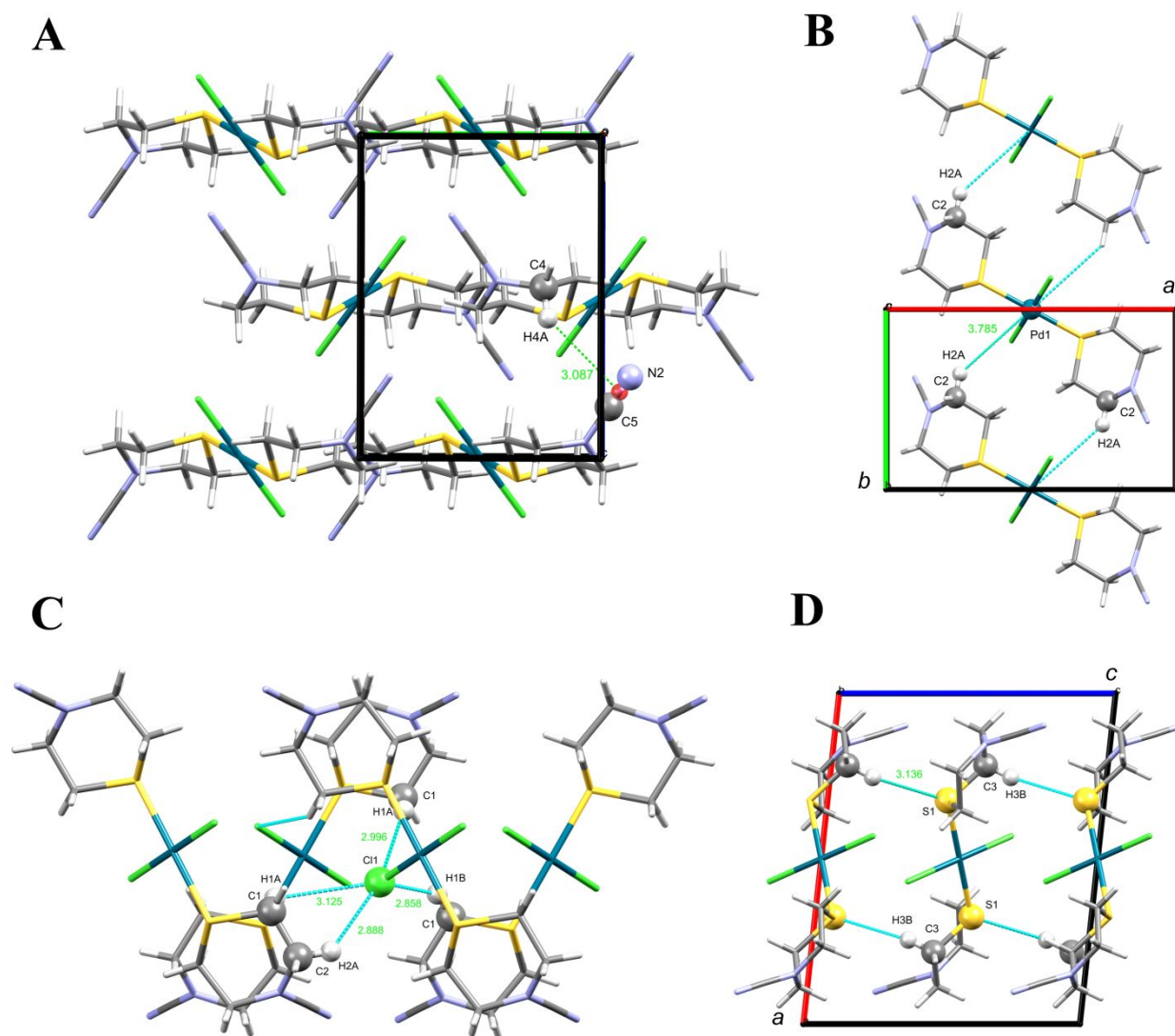


Figure 7. C–H/S (A), C–H/Pd (B), C–H/Cl (C) and C–H/ $\pi$  (D) interactions in the crystal packing of **2**.

Powder XRD measurements (Figure S3, ESI) show that both **1** and **2** crystallize as a pure single phase in the powder. These phases correspond to the single-crystal structures described above. Figure S4 (ESI) shows comparison between experimental powder XRD diffractograms of **1** and **2** with simulated ones of their analogues with different TM-CN conformation of M–S bond with respect to the ring chair conformation. These show that there are significant differences in the powder XRD diffractograms between the two structures with the same metal ion, indicating that a possible mixture of phases would be relatively easily identified in the powder XRD, in particular through appearance of most intensive peaks in 5–10° 2 $\theta$  region. Since experimental powder XRDs (Figures S3 and S4, ESI) do not show any

1 peaks of the second predicted phase, this indicates that **1** and **2** crystallize as a single phase –  
2 axial conformer for Pt(II) and the equatorial one for Pd(II).

3 Since these complexes were obtained as well-formed single crystals, they do not  
4 exhibit any particular observable morphological features that could be correlated to the  
5 energetic effects in their crystal structure (*vide infra*). Images of single crystals from optical  
6 microscope and SEM images of powdered samples used for XRD measurements are shown  
7 in ESI (Figures S5 and S6, respectively).

### 9 ***DFT calculations on solid state periodic and molecular systems***

10 In order to investigate which factors are driving the stability of crystal structures of **1**  
11 and **2** in the solid state, DFT calculations were performed on molecular systems and solid  
12 state periodic systems of Pt and Pd in both axial and equatorial conformers (Table 3).  
13 Optimized structures with axial position of M–S bonds with respect to the TM-CN ring chair  
14 conformation are more stable than the optimized structure with the equatorial position. The  
15 energy difference between axial and equatorial conformers of Pt(II) is slightly larger (3.31  
16 kcal/mol) than in the case of Pd(II) conformers (3.06 kcal/mol). DFT calculations on a  
17 periodic system were conducted using PBE0 functional with norm-conserving  
18 pseudopotential for better accuracy of calculated energies.<sup>48</sup> The results show that the axial  
19 conformer is more stable for Pt(II) complex, while the equatorial one is more stable for Pd(II)  
20 complex (Table 3), which is consistent with experimentally obtained structures, both in the  
21 powder and single crystal experiments. Comparison with the energy differences from the  
22 molecular calculation show the extent of the influence of intermolecular interactions in the  
23 crystal structure. For Pt(II) complex, the preferred conformation does not change, while the  
24 energy difference between axial and equatorial complexes increases by about 18.4 kcal/mol.  
25 On the other hand, for Pd(II) complex, the most stable structure changes from axial to  
26 equatorial, with change in energy difference between two configurations totaling around 5.1  
27 kcal/mol. This suggests that intermolecular interactions in Pt(II) and Pd(II) complexes  
28 stabilize different conformers – axial for Pt(II) and equatorial for Pd(II). In case of Pd(II),  
29 that change is large enough to change the most stable conformation to the equatorial one.

1  
2  
3 Table 3. Lattice parameters and calculated energies for crystal and molecular structures for  
4 equatorial and axial conformers of Pd(II) and Pt(II) complexes. Energy differences between  
5 corresponding structures are shown as  $\Delta E$  (lattice parameters for axial conformers represent  
6 the primitive lattice).  
7  
8  
9

Complex	Space group	$a$ (Å)	$b$ (Å)	$c$ (Å)	$\alpha$ (°)	$\beta$ (°)	$\gamma$ (°)	$\Delta E$ (kcal/mol) crystal	$\Delta E$ (kcal/mol) molecule
1	$I2/a$	10.1930	10.1930	16.0148	48.5	48.5	66.8	0.00	0.00
1-eq	$P2_1/c$	11.4399	7.0711	9.5192	90.00	96.2	90.00	21.70	3.31
2	$P2_1/c$	11.3992	8.2607	10.0984	90.00	94.2	90.00	0.00	0.00
2-ax	$I2/a$	11.2667	11.2667	18.5256	40.7	40.7	56.0	1.96	-3.06

5  
6 ***Hirshfeld surface and fingerprint plot analysis***

7 Hirshfeld surface and fingerprint plot analysis<sup>29,49</sup> allow visualization, quick and easy  
8 understanding of intra- and intermolecular interactions in the crystal structures. Before  
9 calculating the surfaces, the lengths of C–H bonds are normalized to standard values  
10 determined by neutron diffraction. Hirshfeld surfaces and pseudosymmetric 2D fingerprint  
11 plots,<sup>50</sup> existing classical and non-classical interactions and relative contributions to the  
12 Hirshfeld surface for the major intermolecular contacts in the crystal structures of **1** and **2** are  
13 depicted in Figures 8 and 9, respectively. In both complexes the interactions can be observed  
14 in the shape-index plot as red and blue relief regions, as well as in the curvature plot as a flat  
15 zone in the same position of the surface like in the shape-index plot. Regions on the surfaces  
16 through which the complexes interact are marked with white circles.

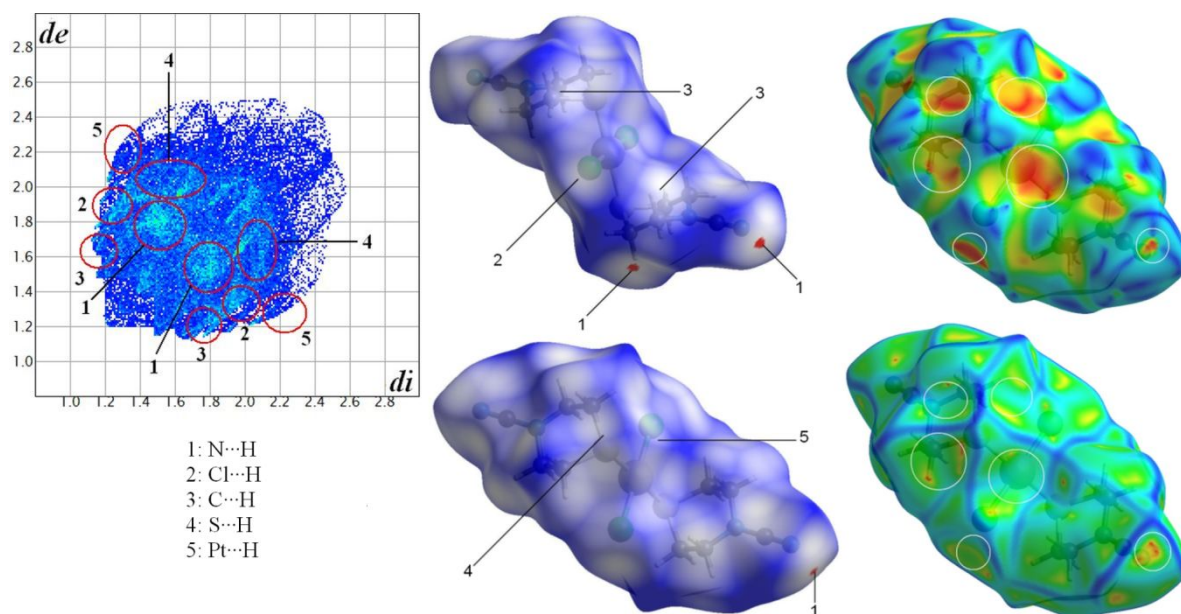


Figure 8. Fingerprint plot, Hirshfeld surfaces mapped with  $d_{\text{norm}}$  (two orientations), shape index and curvedness for **1**.

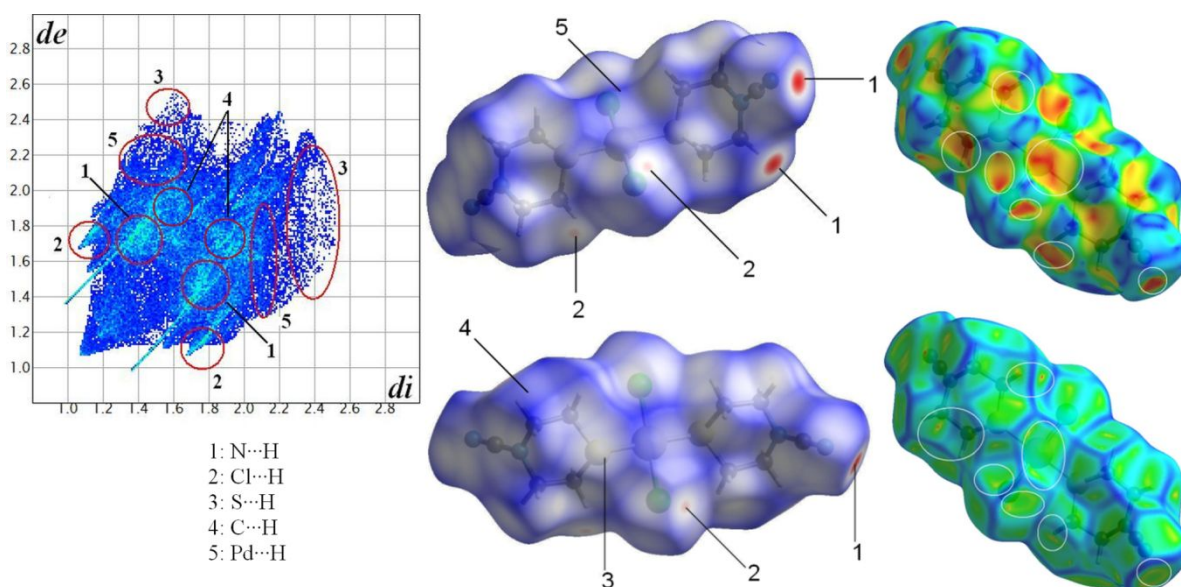


Figure 9. Fingerprint plot, Hirshfeld surfaces mapped with  $d_{\text{norm}}$  (two orientations), shape index and curvedness for **2**.

In the crystal structures, both complexes have the same four main types of interactions, which are within defined  $d_e + d_i$  distances (Table 4). The rest of the contacts that appear in the crystal structures of **1** and **2** are C–H/H and C–H/C contacts. It is apparent that there are some significant differences in interaction distances going from **1** to **2**, like C–H/M

interactions and C–H/N interactions. In addition, there are significant differences in contribution of individual interactions, with C–H/Cl interactions providing much higher contribution in **2**, with shorter interaction distance. In order to investigate these differences and their influence on the structure of individual complexes in more detail, additional DFT calculations were performed on model systems for the four dominant types of interactions (*vide infra*).

Table 4. Overview of the main types of intermolecular interactions obtained from Hirshfeld analysis

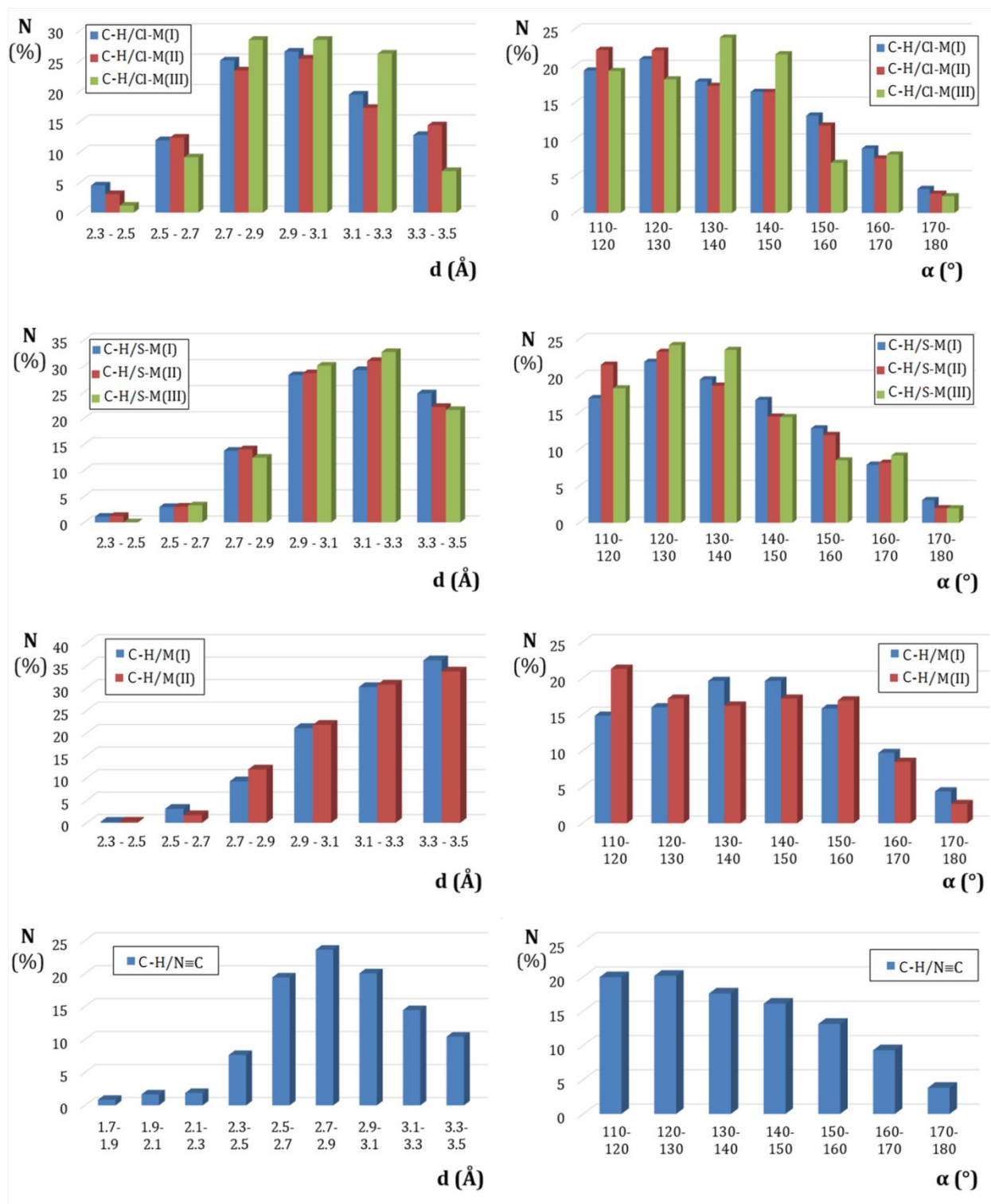
Interactions	$d_e + d_i$ (Å)		Contribution (%)	
	<b>1</b>	<b>2</b>	<b>1</b>	<b>2</b>
C–H/Cl	3.10	2.85	15.6	20.1
C–H/S	3.20	3.30	8.0	5.4
C–H/M	3.40	3.80	1.4	0.8
C–H/N	3.10	2.45	30.1	27.6

#### ***Analysis of C–H/Cl–M, C–H/S–M, C–H/M, and C–H/N≡C interactions***

The study of packing in the crystal structures of **1** and **2** has shown that arrangement of molecules is governed by several non-covalent interactions, where C–H/Cl–M, C–H/S–M, C–H/M, and C–H/N≡C interactions have a significant contribution. In order to describe the geometries of these interactions, a CSD search was performed to gather information about non-covalent interactions.<sup>51</sup> Intermolecular C–H/Cl–M, C–H/S–M, C–H/M, and C–H/N≡C interactions can be characterized as weak hydrogen bonds, because most of the interactions occur at distances larger than 2.5 Å (Figure 10). Of these four types of interactions, the C–H/N≡C and C–H/Cl–M interactions occur at the shortest distance range, while the C–H/M interactions occur at the longest distance range, regardless of the charge of metal ion [M(I), M(II), or M(III)]. Therefore, it can be assumed that the strength of C–H/S–M interactions lies between these interactions. The distributions of  $\alpha$  angle (the angle of the hydrogen bonds) show no tendency towards a linear orientation of interacting species ( $160^\circ \leq \alpha \leq 180^\circ$ ), due to the tendency of interacting species (M, XH, M–Cl, M–S and C≡N groups) to form a



1 simultaneous interactions in the crystal structures over long d distances. This is in agreement  
 2 with previous crystallographic analysis of C–H/X interactions (X = O, N, Cl and F) that  
 3 showed a tendency of most acceptors for nonspecific interactions with many donors.<sup>46</sup> The  
 4 distribution of the  $\alpha$  angle (Figure 10) shows that although there are differences in the trends  
 5 across different interactions and different metal ion charges, they are relatively small.

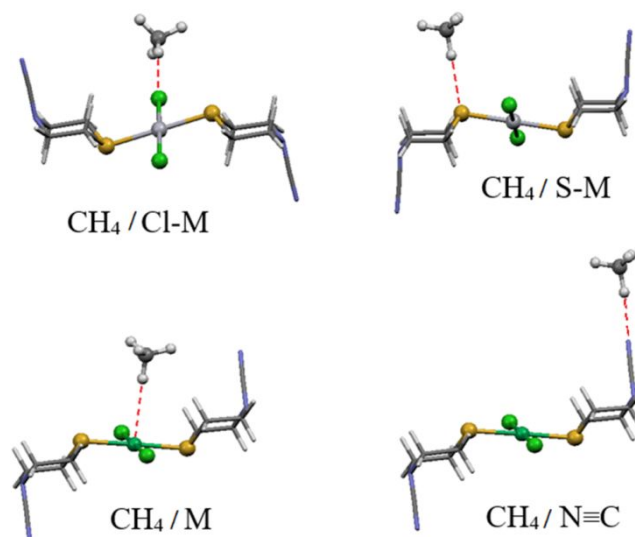


6

1  
2  
3  
4  
5  
6  
7  
8  
9  
10  
11  
12  
13  
14  
15  
16  
17  
18  
19  
20  
21  
22  
23  
24  
25  
26  
27  
28  
29  
30  
31  
32  
33  
34  
35  
36  
37  
38  
39  
40  
41  
42  
43  
44  
45  
46  
47  
48  
49  
50  
51  
52  
53  
54  
55  
56  
57  
58  
59  
60

1 Figure 10. Distributions of  $d$  distances (the length of hydrogen bonds) and  $\alpha$  angles (the angle of the hydrogen bonds) for intermolecular C–H/Cl–M, C–H/S–M, and C–H/M interactions in the crystal structures extracted from CSD.

6 The calculations for prediction of the strength of C–H/Cl–M, C–H/S–M, C–H/M, and C–H/N≡C interactions were performed on model systems (Figure 11) containing CH<sub>4</sub> molecule and [MCl<sub>2</sub>(TM–CN)<sub>2</sub>] complexes (M = Pd, Pt), where M acts as the acceptor in the hydrogen bonding. These calculations were performed only on equatorial conformers, in order to completely isolate individual interactions of the complexes with CH<sub>4</sub>. The results (Figure 12 and Table S4, ESI) show the dependence of the interaction energy on interatomic distance, where C–H/M interactions exhibit significantly higher energy values than other types of interactions. The strength of C–H/M interactions, with maximum values of –2.95 kcal/mol for **1**, and –2.84 kcal/mol for **2** (Table S4, ESI), should make them relevant to crystal packing. The increase in the distance between the C–H group and the metal ion results in the loss of interaction energy, which can be compensated by the increased opportunities for additional interactions.<sup>52</sup>



18  
19  
20  
21  
22  
23

Figure 11. Model systems for energy calculations of C–H/Cl–M (C–H⋯Cl=180°, M–Cl⋯H=180°), C–H/S–M (C–H⋯S=180°, M–S⋯H=109°, Cl–M–S⋯H=90°), C–H/M (C–H⋯M=180°, S–M⋯H=90°, Cl⋯S–M⋯H=90°), and C–H/N≡C (C–H⋯N=180°, C≡N⋯H=180°) interactions (M = Pd, Pt).

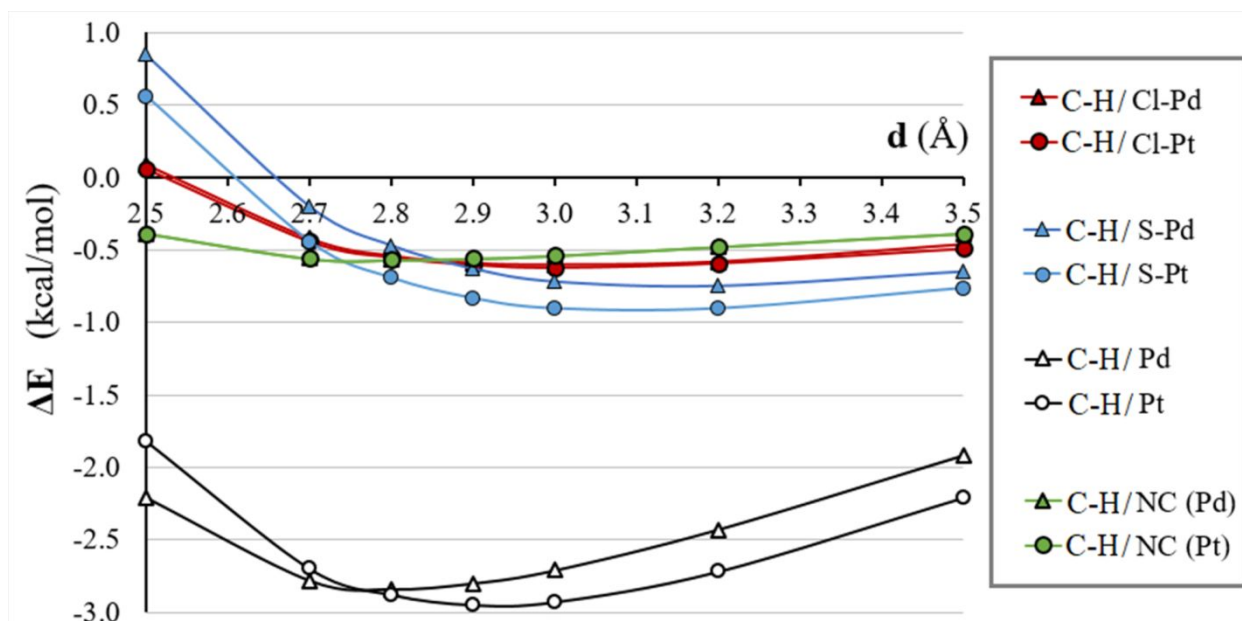


Figure 12. The dependence of the hydrogen bond length ( $d$ ) on the energy of C–H/Cl–M, C–H/S–M, C–H/M and C–H/N≡C interactions (M = Pd, Pt), calculated on  $\text{CH}_4/[\text{MCl}_2(\text{TM-CN})_2]$  model systems at wb97xd/6-31+g\*\* +lanl2dz level of theory.

The interaction strengths of intermolecular interactions from DFT calculation were then calculated for the corresponding distances observed in **1** and **2**, using crystal geometries of axial and equatorial conformers obtained using PBE0 calculations. This suggests that these interactions should play an important role in determining the most stable crystal structure of the corresponding complexes (Table 5). The results show that there is a significant difference in the energy of C–H/M interactions, where shorter Pt–H distance leads to around 1 kcal/mol higher energy of interaction. Coupled with stronger C–H/S interactions in **1**, this indicates that Pt metal center and its immediate surrounding forms considerably stronger hydrogen bonds than Pd, which should be enough to affect the crystal structure of the complex and result in **1** having a different stable crystal structure than **2**. This is in agreement with results of DFT calculations in a periodic system where **1** exhibits shorter C–H/M hydrogen bonds than both the 2-ax and 1-eq (Table S5, ESI). The latter two structures exhibit similar M–H hydrogen bond length as the equatorial conformer of Pd complex. Considering also that the energy difference between two structures of Pt conformers is an order of magnitude larger than the difference between two structures of Pd conformers (Table 5), all of this suggests that the hydrogen bond interactions with the metal center and its immediate surrounding

1 represent a major determining factor in the stability of the crystal structure of **1** and **2**, and  
 2 can be attributed in part for the difference in the crystal structure of these two complexes  
 3 because stronger hydrogen bond interactions appear to favor the axial position of M–S bond  
 4 with respect to the ring chair conformation. On the other hand, Hirshfeld analysis has shown  
 5 a higher contribution of C–H/Cl interactions in **2**, and they have been shown to exhibit longer  
 6 interaction distances (Table 4). This suggests that while **1** is stabilized by hydrogen bonds on  
 7 and around the metal center, **2** is stabilized by interactions with longer distances, which  
 8 afford more opportunities for interactions, rather than stronger individual interactions.

11 Table 5. Interaction strength obtained from the crystal structure distances for **1** and **2**.

Interactions	distances (Å)		Energy (kcal/mol)	
	<b>1</b>	<b>2</b>	<b>1</b>	<b>2</b>
C–H/Cl	3.00	2.90	0.63	0.6
C–H/S	3.20	3.15	0.9	0.75
C–H/M	3.35	3.80	2.5	1.5
C–H/N	2.90	2.75	0.55	0.57

12  
 13  
 14 A calculation of the energies of intermolecular interactions in the crystal structure for  
 15 the axial and equatorial conformers of Pd shows that the intermolecular interactions stabilize  
 16 the equatorial conformer of Pd complex more than its axial counterparts (Table 6). The  
 17 difference in the total energy of intermolecular interactions between two Pd conformers is  
 18 about 10.7 kcal/mol, while the comparison of molecular and crystal structures in DFT  
 19 calculation produced a difference of 5.1 kcal/mol in the relative stability of equatorial  
 20 conformer in molecular and crystal system. This confirms that the interactions between the  
 21 individual molecules in the crystal lattice are the deciding factor in the stability of individual  
 22 crystal structures, rather than the stability of individual molecules that make up the crystal  
 23 lattice.

Table 6. Calculated values of intermolecular interaction energies for different crystal structures of Pd (in kJ/mol unless otherwise noted).

Symmetry operation	R (Å)	electronic	polarization	dispersion	repulsive	Total <i>E</i>
<b>2-axial</b>						
$-y+1/2, -x+1/2, -z+1/2$	10.67	-8.3	-2.5	-9.1	4.4	-15.9
$x, y, z$	11.27	6.7	-0.9	-3.5	0.1	3.4
$x, y, z$	12.39	-18.6	-4.6	-11.9	8.8	-27.9
$-y+1/2, -x+1/2, -z+1/2$	5.15	-17.7	-3.2	-42.1	22.6	-43.8
$x, y, z$	10.58	-1.0	-0.5	-5.1	0.2	-5.8
$-y+1/2, -x+1/2, -z+1/2$	11.76	-15.4	-3.7	-7.3	8	-20.4
Total energy of intermolecular interactions: -110 kJ/mol (-26.4 kcal/mol)						
<b>2-equatorial</b>						
$x, y, z$	13.45	-19.3	-4.5	-21.4	19.5	-30.4
$-x, y+1/2, -z+1/2$	13.33	-17.2	-4	-6	13.4	-18
$x, y, z$	11.44	7.1	-1.6	-6.4	0.7	1.2
$x, y, z$	7.07	-24.7	-9.7	-46.1	46.9	-44.4
$-x, y+1/2, -z+1/2$	5.93	-34.3	-8.9	-47.8	51.7	-52.5
$-x, y+1/2, -z+1/2$	11.63	-6.8	-2.1	-4.9	2.9	-11.2
Total energy of intermolecular interactions: -155 kJ/mol (-37.1 kcal/mol)						

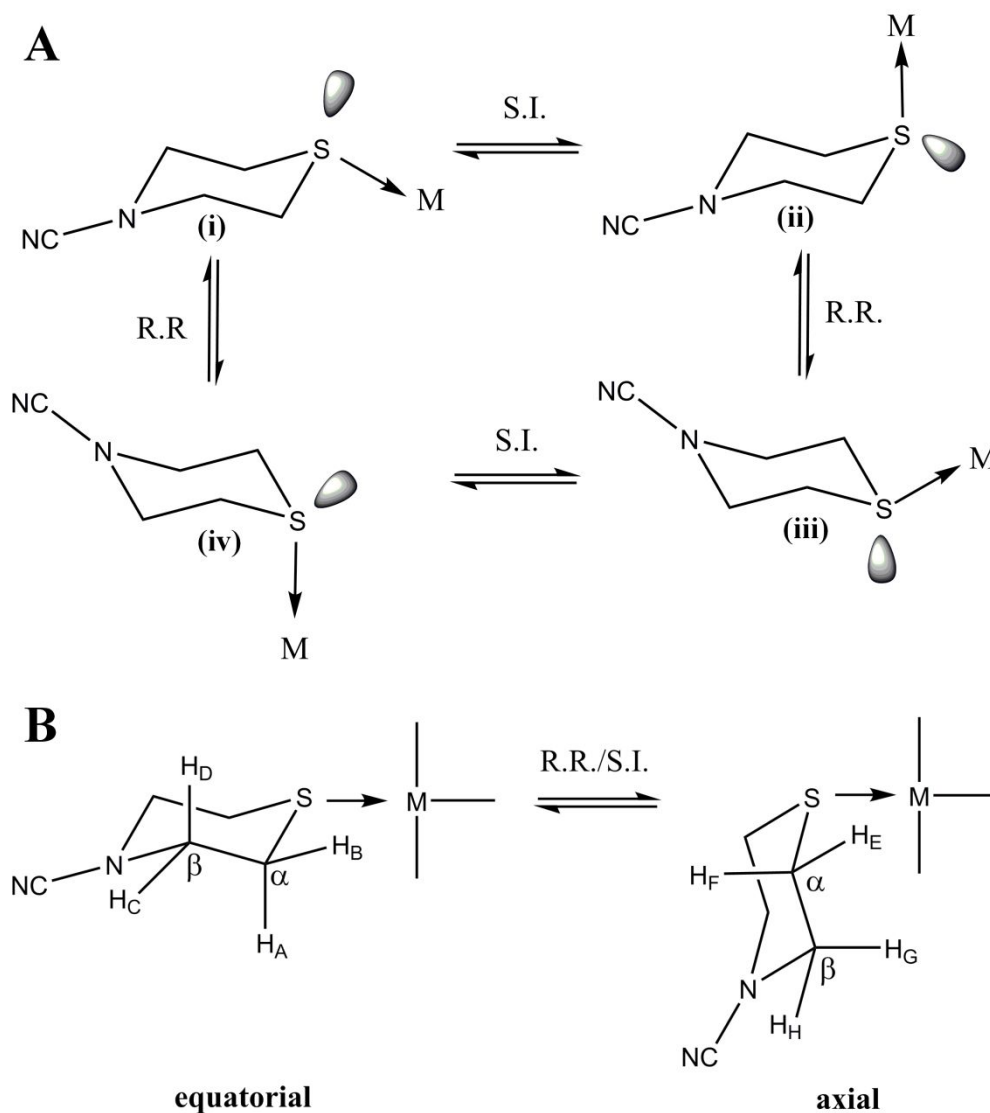
### Solution behavior

NMR spectroscopy was used to study a solution behavior and stability of the complexes. Thus, the NMR spectra of the ligand and the complexes were recorded in two different solvents – DMSO as a solvent with a coordinating ability and capability for a hydrogen bond formation and MeNO<sub>2</sub> as a non-coordinating solvent with a low tendency for hydrogen bond formation. Assignments of signals in <sup>1</sup>H and <sup>13</sup>C NMR spectra of the ligand and the complexes are given in Tables S6 and S7 (ESI).

In the <sup>1</sup>H NMR spectra of TM-CN in both solvents two signals are observed (Figure S7, ESI). A multiplet at a higher field corresponds to the equivalent CH<sub>2</sub> groups which are closer to the sulfur atom (α- and α'-CH<sub>2</sub>), while a lower field signal corresponds to the other two equivalent CH<sub>2</sub> groups (β- and β'-CH<sub>2</sub>). The shape of both signals can be described as a poorly resolved doublet of doublets originating from geminal and trans-diaxial couplings of adjacent CH<sub>2</sub> groups. The <sup>13</sup>C NMR spectra of TM-CN in both solvents (Figure S8, ESI) consist of three absorptions due to the α, β and carbonitrile carbon atoms of the ligand ring.

Analysis and interpretation of NMR spectra of the complexes requires consideration of possible conformations of the complexes. Conformational changes in the case of **1** and **2**

1 can be derived by analogy with a similar system.<sup>53</sup> They are caused by chair to chair reversal  
 2 of TM-CN ring (R.R.) and pyramidal inversion at the coordinated sulfur atom (S.I.) (Scheme  
 3 1A).<sup>53</sup> The total number of conformers of each of the complexes is greater than those  
 4 depicted in Scheme 1A where the conformation of one ligand ring is considered independent  
 5 of the conformation of the other. Since conformers (i) and (iii) where M–S bond is equatorial  
 6 to the TM-CN ring or conformers (ii) and (iv) where the bond is axial (Scheme 1A) cannot be  
 7 distinguished by <sup>1</sup>H NMR spectroscopy,<sup>53</sup> interconversion between averaged conformational  
 8 isomers of the complexes can be represented as in Scheme 1B.



12 Scheme 1. Possible conformations of **1** and **2** (A). Interconversion between averaged  
 13 conformers of **1** and **2** (B). S.I. = Sulfur inversion, R.R. = ring reversal.

1  
2  
3  
4  
5  
6  
7  
8  
9  
10  
11  
12  
13  
14  
15  
16  
17  
18  
19  
20  
21  
22  
23  
24  
25  
26  
27  
28  
29  
30  
31  
32  
33  
34  
35  
36  
37  
38  
39  
40  
41  
42  
43  
44  
45  
46  
47  
48  
49  
50  
51  
52  
53  
54  
55  
56  
57  
58  
59  
60

In  $^1\text{H}$  and  $^{13}\text{C}$  NMR spectra of **1** in  $\text{DMSO-}d_6$  there are two sets of signals, indicating the presence of two species in solution - the free ligand and one complex specie (Figure S9, ESI). It is reasonable to assume that the complex specie in the solution represents the coordination entity where one of the coordinated TM-CN in **1** is replaced by the solvent molecule. In that case, according to the ratio of intensities of the signals in  $^1\text{H}$  NMR spectrum, in  $\text{DMSO-}d_6$  solution the ratio of amounts of free TM-CN and the complex specie is *ca.* 8.8 : 1.2. The existence of the free ligand and the complex specie in the solution is also evidenced by 2D NMR spectra (COSY, NOESY and  $^1\text{H-}^{13}\text{C}$  HSQC, Figure S10–S12, respectively, ESI). In  $^1\text{H}$  and  $^{13}\text{C}$  NMR spectra of **1** in  $\text{CD}_3\text{NO}_2$  there are also two set of signals (Figure S13, ESI). However, in this non-coordinating solvent the ligand dissociation does not occur. Two set of signals thus can be attributed to different conformers of **1**, the axial conformer being the major one. In  $^1\text{H}$  NMR spectra of **1** in both solvents all signals are broad indicating the onset of the conformation shift (Scheme 1B) at a measurable rate on the NMR timescale. Yet, interconversion at room temperature is faster in DMSO probably due to the hydrogen bond formation ability of this solvent.

$^1\text{H}$  NMR spectra of **2** in both solvents comprise of two very broad signals (Figures S14 and S15, ESI). This indicates that at ambient temperature interconversion process is fast, thus the chemical shifts for all  $\alpha$  and all  $\beta$  methylene protons are averaged. The  $^{13}\text{C}$  NMR spectra of **2** (Figure S14 and S15, ESI) consist of three absorptions due to the  $\alpha$ ,  $\beta$  and carbonitrile carbon atoms of coordinated ligand.

## CONCLUSION

Complexes **1** and **2**, with general formula  $[\text{MCl}_2(\text{TM-CN})_2]$ , were obtained by reaction of TM-CN with  $\text{K}_2[\text{MCl}_4]$ , where  $\text{M} = \text{Pt}$  or  $\text{Pd}$ . Both complexes crystallize in the monoclinic crystal system, but in different space groups. In order to determine the factors leading to the different crystal structures with different metal ion, an in-depth theoretical investigation was conducted, examining the structure of two complexes and comparing them with hypothetical structures with the same metal center and different position of M–S bonds with respect to the ligand chair conformation. It was determined that the most stable molecular structure implies the coordination of TM-CN *via* sulfur atom to both Pt(II) and Pd(II) with the axial position of M–S bond in respect to the ligand chair conformation, although the energy differences between two structures were around 3 kcal/mol. This small

1 energy difference proved significant as the calculations in the crystal system revealed that the  
2 most stable conformers were the axial one for **1** and the equatorial one for **2**, corresponding to  
3 the experimentally obtained structures. Comparison of calculations in the molecular and  
4 crystal systems revealed that it is likely that intermolecular interactions stabilize the axial  
5 conformer for Pt(II) and equatorial one for Pd(II), leading to a change in the most stable  
6 conformation from axial to equatorial in the case of Pd(II). This was confirmed using  
7 calculations of intermolecular interaction energy in the crystal, where equatorial Pd(II)  
8 systems exhibited higher values of intermolecular interaction energy than its axial  
9 counterpart. The magnitude of differences in intermolecular energy between the  
10 corresponding axial and equatorial conformers was in general agreement with the results of  
11 DFT calculations in molecular and crystal systems. The strength of individual interactions in  
12 **1** and **2** was calculated using a series of model systems in order to determine the particular  
13 type of interaction responsible for the differences between two metal complexes. The  
14 difference in the crystal structure of two complexes can be attributed in part to the apparent  
15 inability of Pd(II) system to form shorter distance C–H/M interactions in the axial  
16 conformation, where interaction distances remain relatively the same as in the equatorial  
17 conformation, combined with generally weaker C–H/S interactions. The equatorial conformer  
18 is then stabilized by increased opportunities for longer range interactions, like increased  
19 contribution of C–H/Cl interactions, effecting a change in the most stable conformer going  
20 from a molecular to a periodic crystal system.

21

## 22 **ASSOCIATED CONTENT**

### 23 **Supporting information**

24 Supplementary information contains TGA curves, XRPD diffractograms, IR data, structural  
25 parameters, computational results, optical and SEM images and NMR spectra.

26

### 27 **Accession Codes**

28 CCDC 1966912 and 1966913 contain the supplementary crystallographic data for this paper.  
29 These data can be obtained free of charge via [www.ccdc.cam.ac.uk/data\\_request/cif](http://www.ccdc.cam.ac.uk/data_request/cif) or by  
30 emailing [data\\_request@ccdc.cam.ac.uk](mailto:data_request@ccdc.cam.ac.uk), or by contacting The Cambridge Crystallographic  
31 Data Centre, 12 Union Road, Cambridge CB2 1EZ, UK; fax: +44 1223 336033.

32

33

34



## AUTHOR INFORMATION

Corresponding author

\*E-mail: [nenadf@agrif.bg.ac.rs](mailto:nenadf@agrif.bg.ac.rs). Telephone: +381 11 3336685

## ORCID

Predrag Ristić: 0000-0002-7489-6132

Vladimir Blagojević: 0000-0001-8102-989X

Goran V. Janjić: 0000-0002-4138-2637

Marko V. Rodić: 0000-0002-4471-8001

Predrag Vulić: 0000-0002-4806-4551

Morgan Donnard: 0000-0002-9303-4634

Mihaela Gulea: 0000-0002-2945-0078

Agnieszka Chylewska: 0000-0001-7413-1503

Mariusz Makowski: 0000-0002-7342-722X

Tamara R. Todorović: 0000-0002-7740-3639

Nenad R. Filipović: 0000-0003-2982-5324

## Notes

The authors declare no competing financial interest.

## ACKNOWLEDGMENTS

The authors gratefully acknowledge financial support from the Ministry of Education, Science and Technological Development of the Republic of Serbia (Project No. OI 172057).

## REFERENCES

- (1) Allen, F. H. The Cambridge Structural Database: A Quarter of a Million Crystal Structures and Rising. *Acta Crystallogr. Sect. B* **2002**, 58, 380–388. <https://doi.org/10.1107/S0108768102003890>.
- (2) Li, Y.; Lai, Y. H.; Mok, K. F.; Drew, M. G. B. Transition Metal Complexes of 1,3-Bis(Thiomorpholino)Propane: Crystal Structure and Dynamic  $^1\text{H}$  NMR Study. *Inorg. Chim. Acta* **1999**, 285, 31–38. [https://doi.org/10.1016/S0020-1693\(98\)00260-6](https://doi.org/10.1016/S0020-1693(98)00260-6).
- (3) Kim, T. H.; Shin, Y. W.; Jung, J. H.; Kim, J. S.; Kim, J. Crystal-to-Crystal

- 1  
2  
3 1 Transformation between Three CuI Coordination Polymers and Structural Evidence  
4 for Luminescence Thermochromism. *Angew. Chemie Int. Ed.* **2008**, 47, 685–688.  
5 2  
6 3 <https://doi.org/10.1002/anie.200704349>.  
7  
8  
9 4 (4) Kim, T. H.; Shin N, Y. W.; Lee, S. S.; Kim, J. Two-Dimensional Coordination  
10 Polymer of 3-(Methylthio)-1-Thiomorpholinopropan-1-One Propagated by Rhomboid  
11 Cu-I2-Cu Linker. *Anal. Sci. X-ray Struct. Anal. Online* **2006**, 22, x287–x288.  
12 5  
13 6 <https://doi.org/10.2116/analscix.22.x287>.  
14 7  
15  
16  
17 8 (5) Chiang, H.; Kim, T. H.; Park, H.; Kim, J. Crystal Structure of *Catena*-Poly[[Bis(*N*-  
18 Acethylthiomorpholine- $\kappa$  *S*)Copper(I)]- $\mu$ -Iodido]. *Acta Crystallogr. Sect. E*  
19 9  
20 10 *Crystallogr. Commun.* **2017**, 73, 53–55. <https://doi.org/10.1107/S2056989016019794>.  
21  
22  
23 11 (6) Ding, B.; Huang, Y. Q.; Liu, Y. Y.; Shi, W.; Cheng, P. Synthesis, Structure and  
24 12 Magnetic Properties of a Novel 1D Coordination Polymer  $\{[\text{Cu}_2(\text{Amtrz})_4(1,1-\mu$ -  
25 13  $\text{NCS})_2](\text{ClO}_4)_2 \cdot \text{H}_2\text{O}\}_n$ . *Inorg. Chem. Commun.* **2007**, 10, 7–10.  
26 13  
27 14 <https://doi.org/10.1016/J.INOCHE.2006.08.015>.  
28 14  
29  
30  
31 15 (7) Kim, T. H.; Shin, Y. W.; Lee, S. S.; Kim, J. Supramolecular Assembly of One-  
32 16 Dimensional Channels and Two-Dimensional Brick-Wall Networks from Asymmetric  
33 17 Dithioether Ligands and Copper(I) Iodide. *Inorg. Chem. Commun.* **2007**, 10, 11–14.  
34 17  
35 18 <https://doi.org/10.1016/J.INOCHE.2006.09.001>.  
36 18  
37  
38  
39 19 (8) Merkel, M.; Möller, N.; Piacenza, M.; Grimme, S.; Rompel, A.; Krebs, B. Less  
40 20 Symmetrical Dicopper(II) Complexes as Catechol Oxidase Models - An Adjacent  
41 21 Thioether Group Increases Catecholase Activity. *Chem. - Eur. J.* **2005**, 11, 1201–1209.  
42 21  
43 22 <https://doi.org/10.1002/chem.200400768>.  
44 22  
45  
46 23 (9) Lim, M. H.; Lippard, S. J. Fluorescence-Based Nitric Oxide Detection by Ruthenium  
47 24 Porphyrin Fluorophore Complexes. *Inorg. Chem* **2004**, 43, 6366–6370.  
48 24  
49 25 <https://doi.org/10.1021/IC035418N>.  
50 25  
51  
52 26 (10) Poirier, S.; Lynn, H.; Reber, C.; Tailleux, E.; Marchivie, M.; Guionneau, P.; Probert,  
53 27 M. R. Variation of  $\text{M} \cdots \text{H}-\text{C}$  Interactions in Square-Planar Complexes of Nickel(II),  
54 28 Palladium(II), and Platinum(II) Probed by Luminescence Spectroscopy and X-Ray  
55 29 Diffraction at Variable Pressure. *Inorg. Chem.* **2018**, 57, 7713–7723.  
56 28  
57 29  
58 30 <https://doi.org/10.1021/acs.inorgchem.8b00724>.  
59 30  
60

- 1  
2  
3 1 (11) Poirier, S.; Rahmani, F.; Reber, C. Large d–d Luminescence Energy Variations in  
4 Square-Planar Bis(Dithiocarbamate) Platinum( II ) and Palladium( II ) Complexes with  
5 near-Identical MS<sub>4</sub> Motifs: A Variable-Pressure Study. *Dalton Trans.* **2017**, 46, 5279–  
6 5287. <https://doi.org/10.1039/C7DT00545H>.  
7  
8  
9  
10  
11 5 (12) Mitani, M.; Nakano, T.; Fujita, T. Unprecedented Living Olefin Polymerization  
12 Derived from an Attractive Interaction between a Ligand and a Growing Polymer  
13 Chain. *Chem. - A Eur. J.* **2003**, 9, 2396–2403.  
14 <https://doi.org/10.1002/chem.200304661>.  
15  
16  
17  
18 9 (13) Epstein, L. M.; Shubina, E. S. New Types of Hydrogen Bonding in Organometallic  
19 Chemistry. *Coord. Chem. Rev.* **2002**, 231, 165–181. <https://doi.org/10.1016/S0010->  
20 8545(02)00118-2.  
21  
22  
23  
24 12 (14) Chirik, P. J.; Dalleska, N. F.; Henling, L. M.; Bercaw, J. E. Experimental Evidence for  
25  $\gamma$ -Agostic Assistance in  $\beta$ -Methyl Elimination, the Microscopic Reverse of  $\alpha$ -Agostic  
26 Assistance in the Chain Propagation Step of Olefin Polymerization. *Organometallics*  
27 **2005**, 24, 2789–2794. <https://doi.org/10.1021/OM058002L>.  
28  
29  
30  
31  
32 16 (15) Sundquist, W. I.; Bancroft, D. P.; Lippard, S. J. Synthesis, Characterization, and  
33 Biological Activity of Cis-Diammineplatinum(II) Complexes of the DNA Intercalators  
34 9-Aminoacridine and Chloroquine. *J. Am. Chem. Soc.* **1990**, 112, 1590–1596.  
35 <https://doi.org/10.1021/ja00160a044>.  
36  
37  
38  
39  
40 20 (16) Kozelka, J. Agostic and Hydrogen-Bonding X–H...M Interactions Involving a d8  
41 Metal Center: Recent Advances Towards Their Understanding. In *Noncovalent*  
42 *Forces*; Scheiner, S., Ed.; Springer International Publishing: Cham, 2015; pp 129–158.  
43 [https://doi.org/10.1007/978-3-319-14163-3\\_6](https://doi.org/10.1007/978-3-319-14163-3_6).  
44  
45  
46  
47  
48 24 (17) Ayres, J. N.; Ling, K. B.; Morrill, L. C. *N*-Cyanation of Secondary Amines Using  
49 Trichloroacetonitrile. *Org. Lett.* **2016**, 18, 5528–5531.  
50 <https://doi.org/10.1021/acs.orglett.6b02775>.  
51  
52  
53  
54 27 (18) Agilent Technologies UK Ltd. CrysAlisPro Software System. Oxford 2014.  
55  
56 28 (19) Sheldrick, G. M. *SHELXT* – Integrated Space-Group and Crystal-Structure  
57 Determination. *Acta Crystallogr. Sect. A Found. Adv.* **2015**, 71, 3–8.  
58 <https://doi.org/10.1107/S2053273314026370>.  
59  
60

- 1  
2  
3 1 (20) Sheldrick, G. M. Crystal Structure Refinement with *SHELXL*. *Acta Crystallogr. Sect.*  
4 *C Struct. Chem.* **2015**, 71, 3–8. <https://doi.org/10.1107/S2053229614024218>.  
5 2  
6  
7 3 (21) Hübschle, C. B.; Sheldrick, G. M.; Dittrich, B. *ShelXle*: A Qt Graphical User Interface  
8 for *SHELXL*. *J. Appl. Crystallogr.* **2011**, 44, 1281–1284.  
9 4  
10 <https://doi.org/10.1107/S0021889811043202>.  
11 5  
12  
13 6 (22) Spek, A. L. Structure Validation in Chemical Crystallography. *Acta Crystallogr. Sect.*  
14 *D Biol. Crystallogr.* **2009**, 65, 148–155. <https://doi.org/10.1107/S090744490804362X>.  
15 7  
16  
17 8 (23) Groom, C. R.; Bruno, I. J.; Lightfoot, M. P.; Ward, S. C. The Cambridge Structural  
18 Database. *Acta Crystallogr. Sect. B Struct. Sci. Cryst. Eng. Mater.* **2016**, 72, 171–179.  
19 9  
20 <https://doi.org/10.1107/S2052520616003954>.  
21 10  
22  
23 11 (24) Macrae, C. F.; Bruno, I. J.; Chisholm, J. A.; Edgington, P. R.; McCabe, P.; Pidcock,  
24 E.; Rodriguez-Monge, L.; Taylor, R.; van de Streek, J.; Wood, P. A. Mercury CSD 2.0  
25 12  
26 – New Features for the Visualization and Investigation of Crystal Structures. *J. Appl.*  
27 13  
28 *Crystallogr.* **2008**, 41, 466–470. <https://doi.org/10.1107/s0021889807067908>.  
29 14  
30  
31 15 (25) Frisch, M. J.; Trucks, G. W.; Schlegel, H. B.; Scuseria, G. E.; Robb, M. A.;  
32 16  
33 Cheeseman, J. R.; Scalmani, G.; Barone, V.; Petersson, G. A.; Nakatsuji, H.; Li, X.;  
34 17  
35 Caricato, M.; Marenich, A.; Bloino, J.; Janesko, B. G.; Gomperts, R.; Mennucci, B.;  
36 18  
37 Hratchian, H. P.; Ortiz, J. V.; Izmaylov, A. F.; Sonnenberg, J. L.; Williams-Young, D.;  
38 19  
39 Ding, F.; Lipparini, F.; Egidi, F.; Goings, J.; Peng, B.; Petrone, A.; Henderson, T.;  
40 20  
41 Ranasinghe, D.; Zakrzewski, V. G.; Gao, J.; Rega, N.; Zheng, G.; Liang, W.; Hada,  
42 21  
43 M.; Ehara, M.; Toyota, K.; Fukuda, R.; Hasegawa, J.; Ishida, M.; Nakajima, T.;  
44 22  
45 Honda, Y.; Kitao, O.; Nakai, H.; Vreven, T.; Throssell, K.; Montgomery, J. A. Jr.;  
46 23  
47 Peralta, J. E.; Ogliaro, F.; Bearpark, M.; Heyd, J. J.; Brothers, E.; Kudin, K. N.;  
48 24  
49 Staroverov, V. N.; Keith, T.; Kobayashi, R.; Normand, J.; Raghavachari, K.; Rendell,  
50 25  
51 A.; Burant, J. C.; Iyengar, S. S.; Tomasi, J.; Cossi, M.; Millam, J. M.; Klene, M.;  
52 26  
53 Adamo, C.; Cammi, R.; Ochterski, J. W.; Martin, R. L.; Morokuma, K.; Farkas, O.;  
54 27  
55 Foresman, J. B.; Fox, D. J. Gaussian 09, Revision A.02, Gaussian, Inc., Wallingford  
56 28  
57 CT, 2009.  
58 29 (26) Marenich, A. V.; Cramer, C. J.; Truhlar, D. G. Universal Solvation Model Based on  
59 30  
60 Solute Electron Density and on a Continuum Model of the Solvent Defined by the  
Bulk Dielectric Constant and Atomic Surface Tensions. *J. Phys. Chem. B* **2009**, 113,

- 1  
2  
3 1 6378–6396. <https://doi.org/10.1021/jp810292n>.
- 4  
5  
6 2 (27) Gonze, X.; Jollet, F.; Abreu Araujo, F.; Adams, D.; Amadon, B.; Applencourt, T.;  
7 3 Audouze, C.; Beuken, J. M.; Bieder, J.; Bokhanchuk, A.; et al. Recent Developments  
8 4 in the ABINIT Software Package. *Comput. Phys. Commun.* **2016**, 205, 106–131.  
9 5 <https://doi.org/10.1016/j.cpc.2016.04.003>.
- 10  
11  
12  
13 6 (28) Perdew, J. P.; Ernzerhof, M.; Burke, K. Rationale for Mixing Exact Exchange with  
14 7 Density Functional Approximations. *J. Chem. Phys.* **1996**, 105, 9982–9985.  
15 8 <https://doi.org/10.1063/1.472933>.
- 16  
17  
18  
19 9 (29) McKinnon, J. J.; Jayatilaka, D.; Spackman, M. A. Towards Quantitative Analysis of  
20 10 Intermolecular Interactions with Hirshfeld Surfaces. *Chem. Commun.* **2007**, 37, 3814–  
21 11 3816. <https://doi.org/10.1039/b704980c>.
- 22  
23  
24  
25 12 (30) McKinnon, J. J.; Spackman, M. A.; Mitchell, A. S. Novel Tools for Visualizing and  
26 13 Exploring Intermolecular Interactions in Molecular Crystals. *Acta Crystallogr. Sect. B*  
27 14 *Struct. Sci.* **2004**, 60, 627–668. <https://doi.org/10.1107/S0108768104020300>.
- 28  
29  
30  
31 15 (31) Bruno, I. J.; Cole, J. C.; Edgington, P. R.; Kessler, M.; Macrae, C. F.; McCabe, P.;  
32 16 Pearson, J.; Taylor, R. New Software for Searching the Cambridge Structural Database  
33 17 and Visualizing Crystal Structures. *Acta Crystallogr. Sect. B Struct. Sci.* **2002**, 58,  
34 18 389–397. <https://doi.org/10.1107/S0108768102003324>.
- 35  
36  
37  
38  
39 19 (32) Sajan, D.; Binoy, J.; Pradeep, B.; Venkata Krishna, K.; Kartha, V. B.; Joe, I. H.;  
40 20 Jayakumar, V. S. NIR-FT Raman and Infrared Spectra and Ab Initio Computations of  
41 21 Glycinium Oxalate. *Spectrochim. Acta - Part A Mol. Biomol. Spectrosc.* **2004**, 60,  
42 22 173–180. [https://doi.org/10.1016/S1386-1425\(03\)00193-8](https://doi.org/10.1016/S1386-1425(03)00193-8).
- 43  
44  
45  
46  
47 23 (33) Sundari, V.; Nagarajan, G.; Gurumurthy, S.; Valliappan, R. Synthesis,  
48 24 Characterization and Biological Activities of 3,5-Diaryltetrahydro-N-[(Phenylamino)  
49 25 Methyl]-1,4-Thiazine-1,1-Dioxide. *E-Journal Chem.* **2009**, 6, 177–182.  
50 26 <https://doi.org/10.1155/2009/254747>.
- 51  
52  
53  
54  
55 27 (34) Singh, J. S. FT-IR and Raman Spectra, Ab Initio and Density Functional Computations  
56 28 of the Vibrational Spectra, Molecular Geometries and Atomic Charges of Uracil and 5-  
57 29 Methyluracil (Thymine). *Spectrochim. Acta - Part A Mol. Biomol. Spectrosc.* **2015**,  
58 30 137, 625–640. <https://doi.org/10.1016/j.saa.2014.08.060>.

- 1  
2  
3 1 (35) Krueger, P. J.; Jan, J.; Wieser, H. Infrared Spectra: Intramolecular Trans Lone Pair  
4 Interaction with  $\alpha$ -CH Bonds and the Stability of Conformers in Alcohols and Thiols.  
5 *J. Mol. Struct.* **1970**, 5, 375–387. [https://doi.org/10.1016/0022-2860\(70\)80043-6](https://doi.org/10.1016/0022-2860(70)80043-6).  
6  
7  
8  
9 4 (36) Jeffrey, G. A.; Ruble, J. R.; Yates, J. H. Neutron Diffraction at 15 and 120 K and Ab  
10 Initio Molecular-orbital Studies of the Molecular Structure of 1,2,4-triazole. *Acta*  
11 *Crystallogr. Sect. B* **1983**, 39, 388–394. <https://doi.org/10.1107/S010876818300258X>.  
12  
13  
14  
15 7 (37) Teng, F.; Yu, J. T.; Jiang, Y.; Yang, H.; Cheng, J. A Copper-Mediated Oxidative N-  
16 Cyanation Reaction. *Chem. Commun.* **2014**, 50, 8412–8415.  
17  
18  
19 <https://doi.org/10.1039/c4cc03439b>.  
20  
21 10 (38) Chylewska, A.; Sikorski, A.; Ogryzek, M.; Makowski, M. Attractive S $\cdots$  $\pi$  and  $\pi$ - $\pi$   
22 Interactions in the Pyrazine-2-Thiocarboxamide Structure: Experimental and  
23 Computational Studies in the Context of Crystal Engineering and Microbiological  
24 Properties. *J. Mol. Struct.* **2016**, 1105, 96–104.  
25  
26  
27 <https://doi.org/10.1016/j.molstruc.2015.10.032>.  
28  
29  
30 15 (39) Pavia, D. L.; Lampman, G. M.; Kriz, G.S. *Introduction to Spectroscopy*, third ed.;  
31 Saunders College Division, 2001.  
32  
33  
34 17 (40) Appleton, T. G.; Clark, H. C.; Manzer, L. E. The Trans-Influence: Its Measurement  
35 and Significance. *Coord. Chem. Rev.* **1973**, 10, 335–422.  
36  
37  
38 [https://doi.org/10.1016/S0010-8545\(00\)80238-6](https://doi.org/10.1016/S0010-8545(00)80238-6).  
39  
40  
41 20 (41) Kacan, M.; Turkyilmaz, M.; Karabulut, F.; Altun, O.; Baran, Y. Complexation,  
42 Thermal and Catalytic Studies of N-Substituted Piperazine, Morpholine and  
43 Thiomorpholine with Some Metal Ions. *Spectrochim. Acta - Part A Mol. Biomol.*  
44 *Spectrosc.* **2014**, 118, 572–577. <https://doi.org/10.1016/j.saa.2013.09.031>.  
45  
46  
47  
48 24 (42) Shannon, R. D.; IUCr. Revised Effective Ionic Radii and Systematic Studies of  
49 Interatomic Distances in Halides and Chalcogenides. *Acta Crystallogr. Sect. A* **1976**,  
50 32, 751–767. <https://doi.org/10.1107/S0567739476001551>.  
51  
52  
53  
54 27 (43) Bruno, I. J.; Cole, J. C.; Kessler, M.; Luo, J.; Motherwell, W. D. S.; Purkis, L. H.;  
55 Smith, B. R.; Taylor, R.; Cooper, R. I.; Harris, S. E.; et al. Retrieval of  
56 Crystallographically-Derived Molecular Geometry Information. *J. Chem. Inf. Comput.*  
57 *Sci.* **2004**, 44, 2133–2144. <https://doi.org/10.1021/ci049780b>.  
58  
59  
60

- 1  
2  
3 1 (44) Janjić, G. V.; Milosavljević, M. D.; Veljković, D.; Zarić, S. D. Prediction of Strong O-  
4 H/M Hydrogen Bonding between Water and Square-Planar Ir and Rh Complexes.  
5 2  
6 *Phys. Chem. Chem. Phys.* **2017**, 19, 8657–8660. <https://doi.org/10.1039/c6cp08796e>.  
7 3  
8  
9 4 (45) Kozelka, J.; Bergès, J.; Attias, R.; Fraitag, J. O-H···Pt(II): Hydrogen Bond with a  
10 5 Strong Dispersion Component. *Angew. Chemie - Int. Ed.* **2000**, 39, 198–201.  
11 6 [https://doi.org/10.1002/\(SICI\)1521-3773\(20000103\)39:1<198::AID-](https://doi.org/10.1002/(SICI)1521-3773(20000103)39:1<198::AID-)  
12 7 [https://doi.org/10.1002/\(SICI\)1521-3773\(20000103\)39:1<198::AID-](https://doi.org/10.1002/(SICI)1521-3773(20000103)39:1<198::AID-)  
13 8 [https://doi.org/10.1002/\(SICI\)1521-3773\(20000103\)39:1<198::AID-](https://doi.org/10.1002/(SICI)1521-3773(20000103)39:1<198::AID-)  
14 9 [https://doi.org/10.1002/\(SICI\)1521-3773\(20000103\)39:1<198::AID-](https://doi.org/10.1002/(SICI)1521-3773(20000103)39:1<198::AID-)  
15 10 [https://doi.org/10.1002/\(SICI\)1521-3773\(20000103\)39:1<198::AID-](https://doi.org/10.1002/(SICI)1521-3773(20000103)39:1<198::AID-)  
16 11 [https://doi.org/10.1002/\(SICI\)1521-3773\(20000103\)39:1<198::AID-](https://doi.org/10.1002/(SICI)1521-3773(20000103)39:1<198::AID-)  
17 12 ANIE198>3.0.CO;2-O.  
18 13  
19 8 (46) Rizzato, S.; Bergès, J.; Mason, S. A.; Albinati, A.; Kozelka, J. Dispersion-Driven  
20 9 Hydrogen Bonding: Predicted Hydrogen Bond between Water and Platinum(II)  
21 10 Identified by Neutron Diffraction. *Angew. Chemie Int. Ed.* **2010**, 49, 7440–7443.  
22 11 <https://doi.org/10.1002/anie.201001892>.  
23 12  
24 12 (47) Harrison, J. A.; Sajjad, M. A.; Schwerdtfeger, P.; Nielson, A. (Al) J. Multiple Weak  
25 13 C–H Intramolecular Hydrogen Bonding as an Aid to Minimizing Bond Rotation  
26 14 Flexibility. *Cryst. Growth Des.* **2016**, 16, 4934–4942.  
27 15 <https://doi.org/10.1021/acs.cgd.6b00496>.  
28 16  
29 16 (48) Tsipis, A. C. DFT Flavor of Coordination Chemistry. *Coord. Chem. Rev.* **2014**, 272,  
30 17 1–29. <https://doi.org/10.1016/j.ccr.2014.02.023>.  
31 18  
32 18 (49) Spackman, M. A.; McKinnon, J. J. Fingerprinting Intermolecular Interactions in  
33 19 Molecular Crystals. *CrystEngComm* **2002**, 4, 378–392.  
34 20 <https://doi.org/10.1039/b203191b>.  
35 21  
36 21 (50) Maity, T.; Mandal, H.; Bauzá, A.; Samanta, B. C.; Frontera, A.; Seth, S. K.  
37 22 Quantifying Conventional C-H··· $\pi$ (Aryl) and Unconventional C-H··· $\pi$ (Chelate)  
38 23 Interactions in Dinuclear Cu(Ii) Complexes: Experimental Observations, Hirshfeld  
39 24 Surface and Theoretical DFT Study. *New J. Chem.* **2018**, 42, 10202–10213.  
40 25 <https://doi.org/10.1039/c8nj00747k>.  
41 26  
42 26 (51) Britton, D.; Stocker, F. B.; Staeva, T. P. Copper(I) Cyanide-Thiomorpholine (3/1).  
43 27 *Acta Crystallogr. Sect. C Cryst. Struct. Commun.* **1999**, 55, 2014–2016.  
44 28 <https://doi.org/10.1107/S0108270199011622>.  
45 29  
46 29 (52) Ninković, D. B.; Janjić, G. V.; Veljković, D. Ž.; Sredojević, D. N.; Zarić, S. D. What  
47 30 Are the Preferred Horizontal Displacements in Parallel Aromatic-Aromatic

- 1  
2  
3 1 Interactions? Significant Interactions at Large Displacements. *ChemPhysChem* **2011**,  
4 12, 3511–3514. <https://doi.org/10.1002/cphc.201100777>.  
5 2  
6  
7 3 (53) Abel, E. W.; Booth, M.; Orrell, K. G. Determination of the Separate Barrier Energies  
8 4 for Six-membered Ligand Ring Reversal and Pyramidal Sulphur Inversion in  
9 5 Complexes of Palladium(II) and Platinum(II). A Dynamic Hydrogen-1 and Carbon-13  
10 6 Nuclear Magnetic Resonance Study. *J. Chem. Soc., Dalton Trans.* **1980**, 1582–1592.  
11 7 <https://doi.org/10.1039/DT9800001582>  
12  
13  
14  
15  
16  
17 8  
18  
19  
20 9  
21  
22 10  
23  
24  
25 11  
26  
27 12  
28  
29  
30 13  
31  
32 14  
33  
34  
35 15  
36  
37 16  
38  
39  
40 17  
41  
42 18  
43  
44  
45 19  
46  
47 20  
48  
49  
50 21  
51  
52 22  
53  
54  
55 23  
56  
57 24  
58  
59  
60

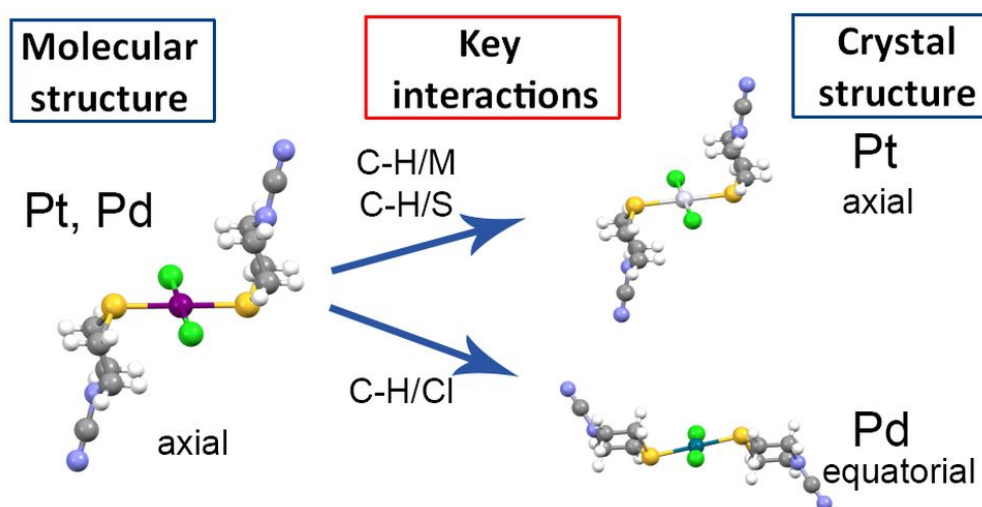


## For Table of Contents Use Only

**The influence of C–H/X (X = S, Cl, N, Pt/Pd) interactions on the molecular and crystal structures of Pt(II) and Pd(II) complexes with thiomorpholine-4-carbonitrile: crystallographic, thermal and DFT study**

Predrag Ristić, Vladimir Blagojević, Goran V. Janjić, Marko V. Rodić, Predrag Vulić,  
Morgan Donnard, Mihaela Gulea, Agnieszka Chylewska, Mariusz Makowski,  
Tamara R. Todorović, Nenad R. Filipović\*

Structural analysis of Pt(II) and Pd(II) complexes with thiomorpholine-4-carbonitrile has shown that Pt-complex exhibits axial, while Pd-complex exhibits equatorial coordination of a sulfur atom with respect to the chair conformation of thiomorpholine-4-carbonitrile ring. The difference can be attributed to the inability of Pd(II) system to form shorter distance C–H/M interactions in the axial conformation, combined with weaker C–H/S interactions.



14